Journal of Hydrology 598 (2021) 126461

Contents lists available at ScienceDirect

Journal of Hydrology

journal homepage: www.elsevier.com/locate/jhydrol

Research papers

A framework for projecting future intensity-duration-frequency (IDF) curves based on CORDEX Southeast Asia multi-model simulations: An application for two cities in Southern Vietnam

Wenpeng Zhao [a,*], Tsuyoshi Kinouchi [a], Hong Quan Nguyen [b,c]

[a] Department of Transdisciplinary Science and Engineering, Tokyo Institute of Technology, Tokyo, Japan
[b] Institute for Circular Economy Development, Vietnam National University, Ho Chi Minh City, Vietnam
[c] Center of Water Management and Climate Change, Institute for Environment and Resources, Vietnam National University, Ho Chi Minh City, Vietnam

ARTICLE INFO

Keywords:
IDF curves
CORDEX Southeast Asia
Bias correction method
Temporal disaggregation
Uncertainty

ABSTRACT

To date, no previous studies based on the Coordinated Regional Climate Downscaling Experiment Southeast Asia (CORDEX-SEA), which represents the most comprehensive set of regional climate model simulations in Southeast Asia, have reported the climate change impacts on Intensity-duration-frequency (IDF) curves for designing urban drainage systems. In this study, a framework to project future IDF curves based on a temporal disaggregation of bias-corrected CORDEX-SEA simulations was developed and applied to two cities in Southern Vietnam, i.e. Ho Chi Minh City (HCMC) and Can Tho City (CTC). First, a new bias correction (BC) method, which we call normalized quantile mapping (NQM), was proposed and compared with two other BC methods, quantile mapping (QM) and quantile delta mapping (QDM), to select a suitable BC method for downscaling each dataset of CORDEX-SEA multi-model simulations. A temporal disaggregation model in an artificial neural network (ANN) framework was introduced to obtain future sub-daily rainfall extremes, and the results were compared with the widely used stochastic model, Hyetosminute. Selecting a suitable BC method for each dataset performs better than using one BC method for all datasets in decreasing the ensemble spread by 47.1% in HCMC and 61.4% in CTC. The temporal disaggregation by ANN performs much better than Hyetosminute in durations shorter than or equal to six hours. IDF curves (based on ensemble mean of seven climate models) projected for the far future period (2066–2085) reveal that the rainfall intensity for 25-yr return period is expected to increase by 27.4–32.6% in HCMC and 55.4–72.8% in CTC (depending on the rainfall duration) from those observed for the historical period (1986–2005), while expected to change by −1.1–11.3% for 2-yr return period.

Generally, more increase of rainfall intensity for rarer rainfall events (especially for longer durations) urges us to update the existing drainage systems for higher return periods. The framework developed in this study can serve as an important reference for studying climate impacts on the urban drainage systems in other cities located in the same region.

1. Introduction

A recent Intergovernmental Panel on Climate Change special report has estimated that human activities have warmed the globe by 1 °C since the pre-industrial period, and at the current rate of temperature increase, global warming is expected to rise further to 1.5 °C between 2030 and 2052 (Hoegh-Guldberg et al., 2018). This rise is likely to occur earlier than foreseen by the Paris Agreement because almost all G20 economies (representing 75% of total 2010 greenhouse gas emissions) are not ambitious enough to implement the agreement or achieve their pledged contributions to the implemented policies (Roelfsema et al., 2020). Previous work has shown that extreme precipitation is expected to increase with global warming at a rate of approximately 7% per degree based on the thermodynamic Clausius–Clapeyron relationship (Trenberth et al., 2003). However, this rate varies across different latitudes and is subject to the water availability (i.e., water supply and demand) of that region (Tabari, 2020; Tabari et al., 2019), which requires a regional climate change study focusing on extreme precipitation. This requirement is crucial for policymakers to decide mitigation and adaptation measures for reducing the negative impacts of global

* Corresponding author at: G5, 4259 Nagata-cho, Midori-ku, Yokohama-shi, Japan.
E-mail address: zhao.w.ae@m.titech.ac.jp (W. Zhao).

https://doi.org/10.1016/j.jhydrol.2021.126461
Received 12 January 2021; Received in revised form 6 May 2021; Accepted 15 May 2021
Available online 19 May 2021

warming, and is imperative in the Southeast Asia (SEA) region, which is vulnerable to extreme precipitation-induced floods due to the poor infrastructure (e.g., urban drainage systems) of many developing countries (Hijioka et al., 2014).

Global climate models (GCMs), as the term suggests, provide information on future extreme precipitation at global scales. The coarse spatial resolution of GCMs (usually greater than 100 km) precludes their direct use at local scales (He et al., 2016; Maraun et al., 2010). To obtain finer spatial resolution information, many researchers have developed dynamical downscaling tools (Hewitson and Crane, 1996; Xu et al., 2019). However, dynamical downscaling is computationally expensive and time-consuming, which often exceeds the capability of institutions in developing countries (Trzaska and Schnarr, 2014). To solve this problem, the World Climate Research Programme has established the Coordinated Regional Climate Downscaling Experiment (CORDEX) (Giorgi et al., 2009; Gutowski and Giorgi, 2020). The Coordinated Regional Climate Downscaling Experiment Southeast Asia (CORDEX-SEA) was initiated in 2013 and represents the most comprehensive set of high-resolution (25 km) regional simulations over SEA (Tangang et al., 2020). Based on these CORDEX-SEA simulations, several papers researching future rainfall have been published. Tangang et al. (2020) evaluated the performance of CORDEX-SEA in simulating mean rainfall over SEA in the historical and future periods. Ge et al. (2019) used six ensemble members of CORDEX-SEA simulations to estimate the changes in extreme precipitation over SEA under the 1.5 °C and 2 °C global warming levels. Based on multi-model simulations of CORDEX-SEA, more intense rainfall events are expected to occur over most of Indochina during the middle of the 21st century (Tangang et al., 2018) and at the end of the 21st century (Supari et al., 2020).

Although these studies have used CORDEX-SEA simulations to project changes in daily rainfall in the future, there are no studies on changes in sub-daily (e.g., hourly) rainfall. More specifically, the changes in rainfall intensity–durationfrequency (IDF) curves, representing the relationship between the rainfall intensity, rainfall duration, and frequency of occurrence, based on CORDEX-SEA simulations are not well understood. IDF curves can be estimated by obtaining rainfall quantiles at different durations separately (Hosseinzadehtalaei et al., 2020) or through a general formula that includes rainfall intensity, duration, and frequency of occurrence in one analytical equation (Koutsoyiannis et al., 1998). Traditionally, this estimation of IDF curves is based on the observed rain gauge dataset for a single location (Liew et al., 2014), and for a large region based on the dataset provided by satellite (Endreny and Imbeah, 2009; Marra et al., 2017), weather radar (Marra et al., 2017; Marra and Morin, 2015; Peleg et al., 2018) and reanalysis products (Cannon and Innocenti, 2019; Hosseinzadehtalaei et al., 2020). However, IDF curves developed by these historical datasets can misrepresent future conditions due to the non-stationarity in rainfall (Srivastav et al., 2014). Therefore, updating IDF curves based on the datasets of projected rainfall in the future period is important for the urban drainage system design in the developing countries in SEA. Regarding the projected rainfall datasets, while the regional climate models (RCMs) with a high resolution are suggested in many studies (Poschlod et al., 2021; Tabari et al., 2016; Tangang et al., 2019), their availability is still limited in SEA. Therefore, the outputs from state-of-the-art RCMs provided by CORDEX-SEA simulations were explored in this study.

In addition to the lack of study on IDF curves based on CORDEX-SEA simulations, most climate change impact studies used the raw outputs without a bias correction. Based on the evaluation of CORDEX-SEA in Tangang et al. (2019), a large discrepancy was found between the statistical properties of observed rainfall and those of modeled rainfall. Tangang et al. (2020) suggested that future studies should focus on removing the model bias provided by CORDEX-SEA simulations due to the parameterization schemes, unresolved process in these climate models, and the systematic model bias that arises from the large-scale atmospheric circulation (Volosciuk et al., 2017). Bias correction (BC) method is a standard practice in removing the systematic model bias because it increases the agreement of modeled variables with observed variables and hence decreases the ensemble spread of modeled variables (Chen et al., 2013a; Wang et al., 2016). Generally, BC method cannot be used in datasets with a large spatial gap (Maraun, 2013), but is reliable for (spatially) downscaling the daily data from RCMs to the local rain gauges with respect to the local distributional and time series characteristics (Ivanov and Kotlarski, 2017). For the climate change impact studies based on CORDEX-SEA simulations, previous studies used BC with quantile mapping (QM) to remove the systematic model bias (Ngai et al., 2020; Trinh-Tuan et al., 2019). The main task of QM is to adjust the cumulative distribution function (CDF) of the modeled variables (e.g., rainfall) to resemble the CDF of observed variables (Gudmundsson et al., 2012). In this way, the statistical properties of modeled variables will resemble those of observed variables. However, QM has been criticized for changing the raw modeled climate change signal (CCS), due to its stationarity assumption (Maraun, 2013; Themeßl et al., 2012) and difficulty of removing the bias in temporal structure (e.g., inter-annual variability and temporal dependence of different variables) (Chen et al., 2013b; Maraun, 2013; Volosciuk et al., 2017). Quantile delta mapping (QDM) (Cannon et al., 2015) and scaled distribution mapping (Switanek et al., 2017) were developed without a stationarity assumption. The nesting BC methods for correcting the bias at multiple temporal scales have shown success in correcting the inter-annual variability (Johnson and Sharma, 2012). Mehrotra and Sharma (2016, 2015) extended the nesting BC methods to simultaneously remove the bias across multiple variables. The results show that considering dependence in multiple variables removes the bias not only in individual variables but also in the correlation between these variables. Cannon (2018) developed the multivariate bias correction algorithm by transferring the statistical properties of multivariate distribution of observed variables to the corresponding multivariate distribution of modeled variables, which showed better accuracy in reproducing the spatio-temporal autocorrelation of rainfall fields. The multivariate bias correction algorithm has also been used for removing the bias in statistical properties and spatial dependence in multiple rain-gauge stations (Su et al., 2020). However, Hnilica et al. (2017) found that the multivariate bias correction algorithm generated unrealistic results when it was applied to variables other than those used for the development of the multivariate bias correction algorithm. Overall, BC methods have been changing from single time scale, variable, and station to multiple time scales, variables, and stations. Even though immense progress has been made in the development of BC methods, different types of assumptions behind these BC methods require us to select suitable BC methods before application (Chen et al., 2013a). This selection is important because the uncertainty associated with the choice of different BC methods is comparable to that associated with the choice of different climate models (Wang et al., 2016). A recent study also suggested that updating IDF curves based on CORDEX simulations should consider the uncertainty of different BC methods (Hosseinzadehtalaei et al., 2020).

Regarding the temporal resolution, few climate models of CORDEX-SEA simulations have provided hourly rainfall products, but most models' temporal resolution is not sufficiently fine to update the IDF curves. Moreover, sub-daily rainfall extremes generated mainly by convective events are not well reproduced by most climate models, such as the models with parameterized convection (Cannon and Innocenti, 2019). Thus, temporal disaggregation tools are needed to obtain rainfall datasets at finer time scales (e.g., hourly rainfall) based on the rainfall datasets at long time scales (e.g., daily rainfall) provided by CORDEX-SEA simulations. Previous studies have often used stochastic models, which generate statistically consistent rainfall events based on stochastic and probabilistic techniques, such as Hyetos (Kossieris et al., 2018; Koutsoyiannis, 2003; Koutsoyiannis and Onof, 2001), Cascade (Müller and Haberlandt, 2018), and MuDrain (Koutsoyiannis, 2003; Lu and Qin, 2014). However, the accuracy of the stochastic models is

closely related to the prior assumption of rainfall generating mechanisms (Kossieris et al., 2018), trade-off between the computational complexity and incorporation of rainfall statistics into the models (Sharma and Mehrotra, 2010). Another category of temporal disaggregation models is based on non-parametric data-driven approaches that quantify the underlying mathematical relation between long-duration and short-duration rainfall without explicit prior physical assumption (Rajagopalan et al., 2010). The method of fragments makes use of the short-duration rainfall information at neighboring stations to disaggregate long-duration rainfall into short-duration fragments at the station of interest (Sharma and Srikanthan, 2006; Poschlod et al., 2018). Burian et al. (2000) and Burian and Durrans (2002) proved that an artificial neural network (ANN) can be a viable way to disaggregate hourly rainfall into sub-hourly rainfall. The data-driven model based on the K-nearest neighbor algorithm was found to perform better than Hyetos in reproducing the hourly rainfall series based on daily rainfall series (Lu and Qin, 2014). Nourani and Farboudfam (2019) proposed several data-driven models, which are especially suitable for rainfall disaggregation in mountainous regions. Mirhosseini et al. (2013, 2014) found that the ANN-based model was better than the stochastic model in reproducing short-duration rainfall extremes, and the stochastic model tended to underestimate the rainfall extremes. Data-driven models such as the ANN-based model are becoming increasingly popular in the field of hydrologic science, owing to more efficient algorithms, higher computing power, and ever-increasing amounts of data (He et al., 2016; Shen et al., 2018).

The objective of this study, therefore, is to project the IDF curves in the future period for designing urban drainage systems in tropical cities based on a temporal disaggregation of bias-corrected climate models provided by CORDEX-SEA simulations. Through this projection, two important aspects are included. First, we propose a new BC method, called normalized quantile mapping (NQM). We evaluate NQM, QM, and QDM by their capabilities of removing the systematic model bias in the historical period and preserving the raw modeled CCS in the future period. Based on this evaluation, we select a suitable BC method for each dataset provided by CORDEX-SEA. Second, for temporal disaggregation, we introduce an ANN-based model to obtain the future (sub-daily) monthly maximum series (MMS) based on the daily datasets provided by CORDEX-SEA.

To our best knowledge, this study is the first to assess the changes in IDF curves in future scenarios based on multi-model simulations of CORDEX-SEA. The proposed BC method, ANN-based temporal disaggregation model, and idea of selecting suitable BC methods can serve as an important reference for climate impact studies in other cities. In this paper, a case study is conducted for Ho Chi Minh City (HCMC) and Can Tho City (CTC). The remainder of this paper is organized as follows. We introduce the research area and present our data in Section 2. The methodology of NQM, ANN-based model, and the method for constructing IDF curves are explained in Section 3. In Section 4, different downscaling and temporal disaggregation methods are compared, final IDF curves are presented, and future works are described; uncertainties in the IDF curves are also discussed. Finally, conclusions are presented in Section 5.

2. Study area and data

2.1. Study area

HCMC, located in the southeastern part of Vietnam, lies approximately 50 km inland from the South China Sea. Over 60% of its administrative area is below 1.5 m above the mean sea level. The region experiences a sub-tropical monsoon climate, with heavy rainfall occurring every year; 90% of this falls during May–November, amounting to approximately 1900 mm. A wide-spread river network covers approximately 16% of the city's area, which ups the water into the urban water systems during high tide levels. HCMC, therefore, is highly vulnerable to flood risk due to the conjunction of high tide levels and heavy rainfall (Vachaud et al., 2019). These two climate factors also account for flooding in CTC (Huong and Pathirana, 2013), which is approximately 131 km away from HCMC. Herein, we focused only on heavy rainfall, as high tide levels are beyond the scope of this study. Apart from these two climate factors, flooding is exacerbated by the rapid urbanization (that affects the infiltration) and poor urban drainage systems (Huong and Pathirana, 2013; Vachaud et al., 2019). Fig. 1 shows the locations of the cities considered for the present study.

2.2. Data

We used two types of rainfall datasets, as summarized in Table 1. Hourly observed rainfall at a single gauging station in each city was provided by the Southern Regional Hydro-Meteorological Center in Vietnam. Given that each city is located in flat terrain, the rainfall observed at a single station can be considered, to a certain extent, valid to represent the statistical rainfall characteristics in each city for the application in urban drainage design. In addition, there is almost no missing value (less than 0.02%) in the observed rainfall series. Daily rainfall for the future periods was provided by all the latest (as of June 2020) CORDEX-SEA simulations (https://esg-dn1.nsc.liu.se/projects/cordex/), except for the one based on the model named IPSL-CM5A-LR_RegCM4-3, which gave an unreasonable underestimation of rainfall in our study area as well as in SEA (Li et al., 2019). The data extracted from the nearest neighboring grid cell center was used for further analysis at the station of interest. For all CORDEX-SEA simulations, we used a high emission scenario (i.e., RCP 8.5), which is viewed as the worst future case in the 21st century (Hausfather and Peters, 2020).

3. Methods

3.1. Procedure

Fig. 2 demonstrates the procedure for constructing the IDF curves.

1: Historical IDF curves (1986–2005) were constructed based on the rainfall quantiles (at different durations) of observed rainfall.

2: A new BC method, NQM, was proposed and compared with QDM and QM. Based on this comparison, we selected a suitable BC method for each dataset provided by the CORDEX-SEA simulations.

3: Selected BC methods were applied to downscale the future daily rainfall datasets projected for the periods of 2026–2045 and 2066–2085.

4: We compared two temporal disaggregation models based on how well they reproduce the observed MMS.

5: We generated sub-daily MMS from the downscaled daily rainfall in step 3 based on the superior disaggregation method in step 4.

6: IDF curves for the future periods were constructed based on the 'change factor' operation mentioned in detail in Section 3.5. The uncertainties in the projected IDF curves were also discussed.

3.2. Normalized quantile mapping

In this section, a new BC method, NQM, was proposed and compared with QM and QDM. Fig. 3 illustrates how to remove the bias at a given empirical cumulative distribution function (ECDF) (quantile of order 0.9 in this figure) by QM, QDM, and NQM. In QM, the error correction value is the ratio of the raw historical model to the observations at ECDF $\approx$ 0.93. This error correction value remains the same between the raw future model and future downscaled data (that is called 'BC by QM', which represents the bias-corrected or downscaled future data by QM) at ECDF = 0.9. Thus, QM uses the error correction values established at a higher ECDF to remove the bias at a lower ECDF, which could alter the raw modeled CCS (Switanek et al., 2017). In QDM, the error correction value is the ratio of the raw future model data to the raw historical model data at ECDF = 0.9. This error correction value multiplied by

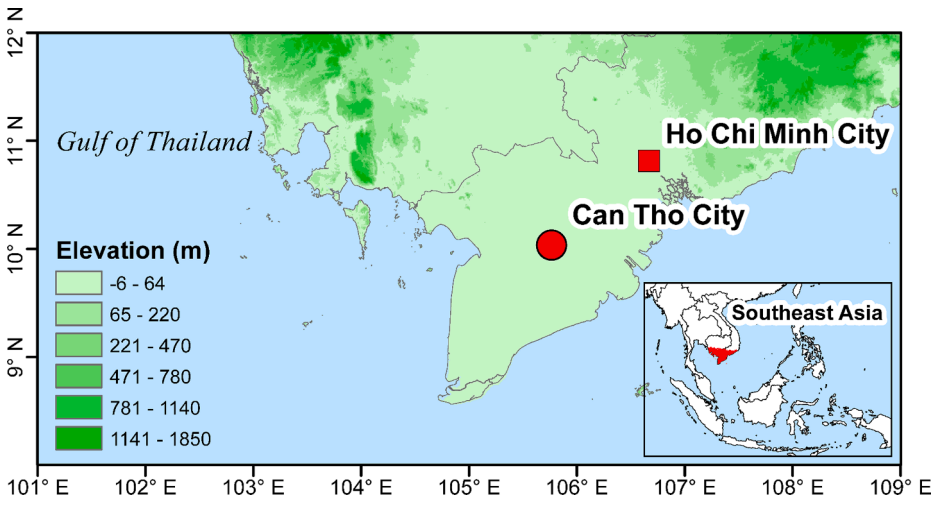

Fig. 1. Location of HCMC and CTC.

Table 1
Datasets used in this study. The index of CORDEX-SEA is listed in the first column.

No.	Dataset (Developer)	Resolution	Time
1	EC-EARTH_RegCM4-3 (ICTP[1])	0.22°(daily)	1986–2005 (Historical period). 2026–2045 (Near future period), 2066–2085 (Far future period)
2	NorESM1-M_REMO2015 (GERICS[2])		
3	MPI-ESM-MR_RegCM4-3 (ICTP)		
4	HadGEM2-ES_REMO2015 (GERICS)		
5	MPI-ESM-LR_REMO2015 (GERICS)		
6	HadGEM2-ES_RCA4 (SMHI[3])		
7	GFDL-ESM2M_RegCM4-3 (ICTP)		
–	Observations (SRHMC[4])	Point (hourly)	1986–2005 (Historical period)

[1] The Abdus Salam International Centre for Theoretical Physics (ICTP).
[2] Climate Service Center Germany (GERICS).
[3] Swedish Meteorological and Hydrological Institute (SMHI).
[4] Southern Regional Hydro-Meteorological Center (SRHMC).

observations is the 'BC by QDM' ('BC by QDM' = observations × raw future model / raw historical model).

QM and QDM assume that biases between the observations and the raw historical model exist at the same ECDF. In other words, the largest (second-largest,…, smallest) observed and modeled quantiles correspond to the same ECDF, which is unverifiable (Switanek et al., 2017). In contrast, in NQM, we determine the location of biases (the way to connect raw historical model and observations) based on a data normalization in step (1) below. This data normalization is used to change the values to a common scale, which is frequently applied in machine learning.

The methodology for applying NQM is explained as follows. Steps (1), (2), and (3) were used to remove the biases of the wet-day rainfall amount and correspond to the three arrow lines, in turn, in Fig. 3 (NQM). We removed the biases of the wet-day frequency in step (4). Step (5) was used to obtain the bias-corrected datasets.

Step (1): set a threshold as the daily minimum observed rainfall amount. Herein, we used 0.1 mm as the threshold, below which all raw modeled rainfall values were set to 0 mm. Next, observations (wet-day) and raw historical model variable (wet-day) were normalized by:

$$\widehat{P}_{OBS} = \frac{P_{OBS} - \bar{P}_{OBS}}{\sigma(P_{OBS})}; \widehat{P}_{M,H} = \frac{P_{M,H} - \bar{P}_{M,H}}{\sigma(P_{M,H})} \quad (1)$$

where the subscripts OBS and M,H denote the observed and modeled variables (rainfall) in the historical period, respectively. P_{OBS} represents the observations (wet-day) and $P_{M,H}$ represents the raw historical model data (wet-day). $\bar{P}$ and $\sigma(P)$ are the mean and standard deviation values of the respective datasets (i.e., observations and raw historical model data). Thus, $\widehat{P}_{OBS}$ and $\widehat{P}_{M,H}$ are the normalized variables. Next, $\widehat{P}_{OBS}$ is mapped into the range of $\widehat{P}_{M,H}$ by:

$$K = \frac{max\left(\widehat{P}_{M,H}\right) - min\left(\widehat{P}_{M,H}\right)}{max\left(\widehat{P}_{OBS}\right) - min\left(\widehat{P}_{OBS}\right)}$$

$$\Delta = K \times \left(\widehat{P}_{OBS} - max\left(\widehat{P}_{OBS}\right)\right) + max\left(\widehat{P}_{M,H}\right) \quad (2)$$

where max (min) is the maximum (minimum) value of the respective datasets. K is the ratio of $\widehat{P}_{M,H}$'s range to $\widehat{P}_{OBS}$'s range. Δ is the location of $\widehat{P}_{OBS}$ in the range of $\widehat{P}_{M,H}$. Then, we linked the observations to the raw historical model by:

$$P^*_{OBS} = \Delta \times \sigma(P_{M,H}) + \bar{P}_{M,H} \quad (3)$$

where P^*_{OBS} is the location of P_{OBS} in the range of $P_{M,H}$. In other words, Eq. (3) gives the location of biases between observations and raw historical model data.

Step (2): remove the biases by error correction values, which are the ratio of the future model data to the historical model data at the same ECDF:

$$\widehat{P}_{BC} = F^{-1}_{M,F}\left(F_{M,H}(P^*_{OBS})\right) \quad (4)$$

where the subscripts BC and M,F denote the bias-corrected and uncorrected modeled variables (rainfall) in the future period, respectively. $\widehat{P}_{BC}$ is the bias-corrected future data with a scaling factor, which is explained in Eq. (5). $F_{M,H}$ is the ECDF of climate model outputs for the historical period. $F^{-1}_{M,F}$ is the inverse ECDF of the climate model outputs for the future period.

Step (3): obtain bias-corrected future data P_{BC} by removing the scaling factor.

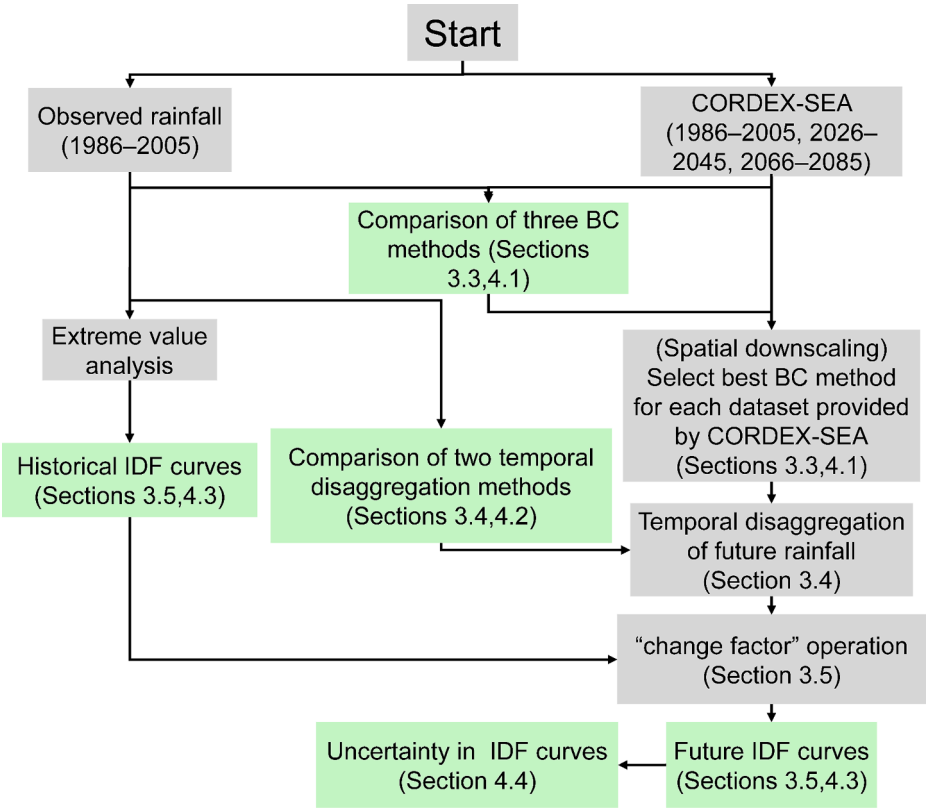

Fig. 2. A flow chart of the studied framework.

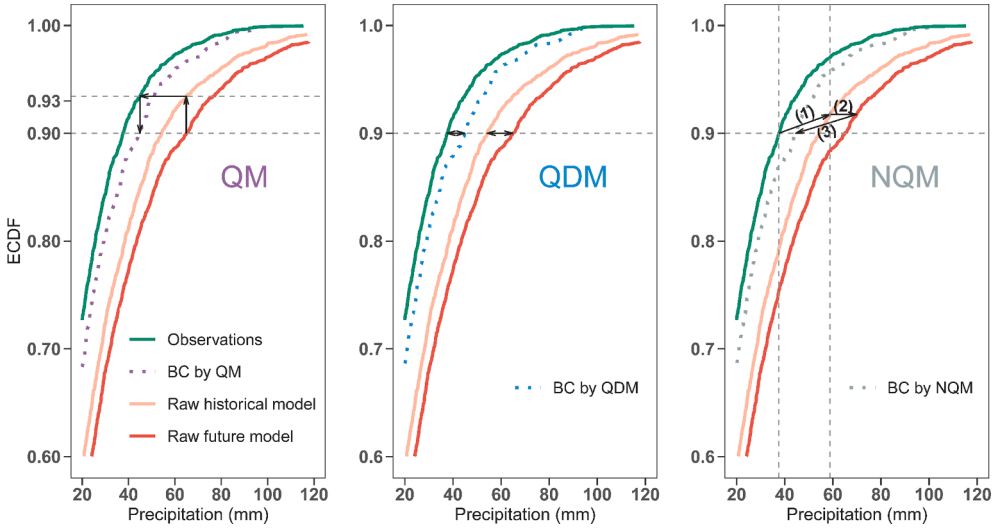

Fig. 3. Difference between the QM, QDM, and NQM methodologies. BC by QM (QDM, NQM) represents the bias-corrected (or downscaled) future projection by QM (QDM, NQM). Raw historical and future models represent climate model outputs (uncorrected outputs) for the historical and future periods, respectively. ECDF represents the empirical cumulative distribution function. '(1)', '(2)', and '(3)' in NQM correspond to the steps (1), (2), and (3) in Section 3.2.

$$P_{BC} = \left(\frac{\frac{\widehat{P}_{BC} - \bar{P}_{M,H}}{\sigma(P_{M,H})} - max\left(\widehat{P}_{M,H}\right)}{K} + max\left(\widehat{P}_{OBS}\right) \right) \times \sigma(P_{OBS}) + \bar{P}_{OBS} \quad (5)$$

Eq. (5) is the inverse operation of Eqs. (1), (2), and (3).

Step (4): remove the biases of the wet-day frequency based on Switanek et al. (2017):

$$WD_{BC} = WD_{M,F} \times \frac{WD_{OBS}/TD_{OBS}}{WD_{M,H}/TD_{M,H}} \quad (6)$$

where *WD* and *TD* are the number of wet days and the total number of days including dry days (days without rainfall), respectively. For example, let's assume that the total number of days was 1840 for the observed data, raw historical, and future model data, while those of wet days were 1339, 1714, and 1706, respectively. Based on step (4), WD_{BC} was found to be 1706 × (1339/1840) / (1714/1840) = 1333 days (1333

is the nearest integer value).

Step (5): place the bias-corrected future wet-day series back into the raw future model wet-day series in the correct temporal locations.

BC methods adjust the CDF of the modeled variables (e.g., rainfall) to resemble the CDF of observed variables (Gudmundsson, 2012). However, CDF only considers the datasets in ascending or descending order and does not consider the temporal structure (e.g., inter-annual variability) of the datasets. Therefore, in step (5), we sorted the bias-corrected datasets in the same order (or rank) as the raw future model datasets. In the previous example, based on steps (1), (2), and (3), we obtained a bias-corrected future wet-day series with a length of 1339. This length was different from 1333 in step (4). Therefore, first, the smallest 6 (1339–1333 = 6) rainfall values in this wet-day series were all set to 0 mm. Second, the maximum daily rainfall in the raw future model was found to occur on September 13, 2040. Thus, the maximum bias-corrected rainfall was reinserted on that day. Third, a similar operation was performed for the rest of the 1332 (1333–1 = 1332) bias-corrected rainfall values. When the number of wet days from step (4) (1240) was larger than that from steps (1), (2), and (3) (1232), we selected 1240 from step (4) as the wet-day frequency. In this case, the largest 8 (1240–1232) rainfall values of the smallest 598 (1840–1232) raw future model rainfall values were placed in the correct temporal locations. Herein, we performed bias correction on a seasonal basis by grouping the datasets into different seasons (seasonal moving window), as suggested by Räty et al. (2014) because this can consider seasonality, or a monthly moving window if a longer duration of the observed rainfall is available.

3.3. Comparison of NQM, QDM, and QM

Two steps were followed to compare NQM, QDM, and QM. Firstly, we compared the reproducibility of the upper 95th percentile of the wet-day rainfall series (Q95th) by each method based on the observed datasets. Secondly, we compared how each method preserves the raw modeled CCS of CORDEX-SEA in Q95th in the future period. Q95th is a commonly used index for climate change impact studies focusing on rainfall extremes (Chen et al., 2013a). The quantile is calculated based on the default method in *quantile function* in R language. The details of these steps are described as follows.

In the first step, we chose 1986–1995 as the calibration period and 1996–2005 as the validation period. Each BC method was calibrated using the data for 1986–1995 and the systematic model bias was removed considering the data for 1996–2005. Then, we compared the bias-corrected model values with the observed values obtained for 1996–2005. Specifically, the comparison was represented by the relative error through $100\%*(Q95th_{BC} - Q95th_{OBS})/Q95th_{OBS}$. $Q95th_{BC}$ and $Q95th_{OBS}$ represent the Q95th of bias-corrected wet-day rainfall series and observed wet-day rainfall series, respectively.

In the second step, we checked how each BC method preserves raw modeled CCS in Q95th in future periods (2026–2045 and 2066–2085). For example, the raw future model showed a 20% increase in Q95th from the raw historical model. If the bias-corrected dataset showed a 10% increase in Q95th from the observed dataset, the relative change of raw modeled CCS was 100% × (10%–20%)/20% = −50%. These two steps were similar to Cannon et al. (2015) and Chen et al. (2013a). For each BC method, we set a threshold = 0.1 mm, below which all modeled values were set to zero. QDM and QM were implemented by R packages *MBC* and *qmap* respectively, that are available online (https://cran.r-project.org/web/packages/). For each bias-corrected model, we recorded the mean values of relative error and relative change.

To select a suitable BC method for each dataset from CORDEX-SEA, results based on the previous two steps were combined. First, we rescaled the relative error series and relative change series as follows:

$$X^* = 100\% \times \frac{|X| - |X_{min}|}{|X_{max}| - |X_{min}|} \quad (7)$$

where $|X|$, $|X_{max}|$, and $|X_{min}|$ denote the absolute value of the data series (that is the relative error series or relative change series), maximum of this series, and minimum of this series, respectively. X^* denotes the mapped data series. Second, we took the average of the mapped relative error series and the mapped relative change series. This average is called the total error and is used for selecting a suitable BC method for each dataset from CORDEX-SEA in each station. This selection is to improve the accuracy of each ensemble member by considering the influence of bias correction and CCS preservation through Eq. (7), and thus reduce uncertainty in the ensemble mean and spread. These three BC methods implicitly conduct spatial downscaling, which has been applied in several studies for climate change impacts (Chen et al., 2018, 2014; Ivanov and Kotlarski, 2017; Li et al., 2017; Li and Babovic, 2019; Lima et al., 2018; Mullan et al., 2016).

3.4. Temporal disaggregation model

For temporal disaggregation, we introduced an ANN-based model that is used to obtain future sub-daily MMS based on daily rainfall datasets provided by CORDEX-SEA simulations. This ANN-based model is similar to the temporal disaggregation model used in Mirhosseini et al. (2014), which is used to reproduce MMS instead of the whole sub-daily rainfall series; However, there are two important advancements: (1) Instead of using all rainfall data information, we only extracted the extreme rainfall information for training, which is more computationally efficient, (2) to improve accuracy, we used the most accurate outputs simulated in previous steps (for 12 hourly rainfall) as the inputs for later steps (for 6, 18 and 24 hourly rainfall). For comparison, we applied a widely used stochastic disaggregation model called Hyetos (Koutsoyiannis, 2003). Hyetos was improved by Kossieris et al. (2018), as it allowed for a temporal disaggregation from daily scale down into 1-min scale. This model is called Hyetosminute, which was implemented in this study using the R package (http://www.itia.ntua.gr/en/softinfo/3/).

More details on how to apply Hyetosminute and ANN-based model are described as follows. Hyetosminute was used for generating hourly rainfall series based on daily rainfall series. Hyetosminute, as a stochastic model, generates statistically consistent hourly rainfall events, thus needing suitable distribution functions to simulate the rainfall duration and intensity. The cell (rainfall events divided into different cells) intensity was simulated by Weibull distribution, which was also suggested by Kossieris et al. (2018). A preliminary analysis showed that a model considering dependence between cell duration and intensity performed better, which was similar to Kossieris et al. (2018). For the ANN-based model, we used a three-layered (input, hidden, and output layer) back-propagation network. The input layer sends the input variable (shown in Table 2) to the hidden layer (that produces the output variable based on nonlinear transformations), and the output layer gives the output variable (Burian et al., 2000). The objective of back-propagation is to minimize the error function (the mean squared error in our study) by adjusting the nonlinear transformations (Burian et al., 2000). We applied 20 hidden neurons with a dropout (rate = 0.5) between the hidden layer and output layer based on trial and error. Dropout is a technique where selected neurons are ignored randomly in the training to avoid overfitting. Such settings are problem-dependent and are based on a trial rule (Macukow, 2016; Mendenhall and Meiler, 2016). The input and output variables are listed in Table 2. Monthly maximum 1, 3, 6, 12, 18, 24 hourly rainfall series are signified by MMR1, MMR3, MMR6, MMR12, MMR18, MMR24, respectively. The optimum input variable was selected based on the minimum Akaike Information Criterion (AIC), which is widely used for input variable selection (Mirhosseini et al., 2014; Panchal et al., 2010). To set up the model, 80% of the datasets were used for training (80%) and validation for minimizing over-fitting (20%), and the remaining 20% for testing (Mirhosseini et al., 2014). For example, among 20-year observed hourly

Table 2
Selecting the optimum input variables for ANN-based models based on Akaike Information Criterion (AIC). Output variables MMR1, MMR3, MMR6, MMR12, MMR18, and MMR24 represent monthly maximum 1, 3, 6, 12, 18, and 24 hourly rainfall series, respectively. P is the total rainfall in that particular day (t) and month (m). P_{t-1} and P_{t+1} are the daily rainfall centered by t. *sim_MMR*12 is the disaggregated MMR12 in that month. The best input variables are selected for each output variable based on the minimum AIC value (shown by the bold number).

Station	Input variable	Output variable					
		MMR1	MMR3	MMR6	MMR12	MMR18	MMR24
HCMC	$(P_{t-1}, P_t, P_{t+1}, P_m, sim\_MMR12)$	4.69	4.47	4.36	None	4.42	4.64
	$(P_{t-1}, P_t, P_{t+1}, sim\_MMR12)$	4.75	4.44	**4.25**	None	**4.29**	**4.57**
	$(P_{t-1}, P_t, P_{t+1}, P_m)$	**4.42**	4.11	4.47	3.90	4.50	4.68
	(P_{t-1}, P_t, P_{t+1})	4.54	**4.09**	4.29	**3.62**	4.37	4.65
CTC	$(P_{t-1}, P_t, P_{t+1}, P_m, sim\_MMR12)$	3.85	4.48	4.64	None	3.57	3.16
	$(P_{t-1}, P_t, P_{t+1}, sim\_MMR12)$	4.12	4.36	**4.61**	None	**3.53**	**3.05**
	$(P_{t-1}, P_t, P_{t+1}, P_m)$	**3.65**	4.33	4.66	3.46	4.04	3.74
	(P_{t-1}, P_t, P_{t+1})	4.10	**4.28**	4.74	**3.41**	4.01	3.61

rainfall series, we used 154 (12 months × 20 years × 80% × 80%) observed MMR1 as the output variable for training. Based on the observed MMR1, we knew the exact time (i.e., month (m), day (t), the previous day ($t-1$), the next day ($t+1$)) when MMR1 occurred and the amount (P) of rainfall accumulated during these times. Then, we had 154 sets of $(P_{t-1}, P_t, P_{t+1}, P_m)$ as the input variable. We also found that the ANN-based model simulated MMR6, MMR18, and MMR24 better if we used simulated MMR12 (*sim_MMR*12) as the input variable. Other combinations of input variables, such as $(P_{t-2}, P_{t-1}, P_t, P_{t+1}, P_m, sim\_MMR24)$, performed worse than those in Table 2 and are not shown here. Overall, we established 12 ANN-based models for six durations at two stations.

Table 2 shows that if we use the ANN-based model, we need to know the exact time when sub-daily rainfall extremes (e.g., MMR1) occurred. This information is unavailable in the future daily rainfall series provided by CORDEX-SEA. Therefore, firstly, we regarded daily rainfall as P_t and obtained 7305 (7305 days during 2026–2045 or 2066–2085) sets of $(P_{t-1}, P_t, P_{t+1}, P_m)$. Secondly, $(P_{t-1}, P_t, P_{t+1}, P_m)$ was input into ANN-based model to generate 7305 output variables. Next, we exacted MMS from these output variables. This procedure was also tested in the historical period (Section 4.2).

3.5. Constructing IDF curves

For the historical period, extreme value analysis (EVA) was conducted using the annual maximum series (AMS) given from the observed rainfall series. For the future period, EVA was applied to AMS extracted from MMS, which is the product of downscaling and temporal disaggregation explained in Sections 3.3 and 3.4, to determine the return rainfalls (representing the rainfall intensity with a given return period) at different durations that were later used to construct the IDF curves. Compared with the peak over threshold method, the AMS method can ensure the independence of the data series and is suitable for the EVA in highly variable climatic conditions (Marra et al., 2017). For EVA, we applied a Bayesian generalized extreme value (GEV) distribution model proposed by Lima et al. (2018) based on the scaling-invariant property of the rainfall process (Blanchet et al., 2016; Koutsoyiannis et al., 1998). Lima and coworkers applied this model for estimating GEV parameters at several stations in a homogeneous hydrologic region simultaneously, while we used it for HCMC and CTC, separately. The scaling-invariant property implies that the statistical properties of rainfall with different rainfall durations are linked to each other by an operator consisting of the scaling ratio and scaling exponent (Blanchet et al., 2016). GEV has been widely used to fit the annual maxima in the field of hydrology (Coles et al, 2001; Papalexiou et al., 2013). The standard cumulative distributing function of GEV is defined by:

$$G(y) = exp\left\{ -\left[1 + \xi\left(\frac{y-\mu}{\sigma}\right)\right]^{-\frac{1}{\xi}} \right\}, \text{for}, \left\{ y : 1 + \xi\left(\frac{y-\mu}{\sigma}\right) > 0 \right\} \quad (8)$$

where $-\infty < \mu < \infty, \sigma > 0$ and $-\infty < \xi < \infty$. $\mu, \sigma,$ and ξ are the location, scale, and shape parameters of GEV, respectively. y denotes the rainfall intensity data.

There are mainly two methods for parameter estimation based on the likelihood function: the maximum likelihood method and the Bayesian method (Muller et al., 2008). The Bayesian method is desirable since it can reasonably assess the uncertainty in estimated parameters (Mélèse et al., 2018). Moreover, to reduce the uncertainty arising from the scarcity of data, Bayesian method can include other sources of information through the prior distributions of parameters (Muller et al., 2008). The joint posterior distribution for each station with the complete parameter set Θ of the Bayesian GEV model is given by (Lima et al., 2018):

$$\begin{gathered} Pr\left(\frac{\Theta}{y}\right) \propto \prod_{j=1}^{T} \prod_{d=1}^{24} GEV\left(y_{d,j} | \mu_d, \sigma_d, \xi_d\right) \times \\ N\left(log(\mu_d) | \alpha - H \cdot log\left(\frac{d+\theta}{d_{24}+\theta}\right), \tau_\mu^2\right) \times N\left(log(\mu_d) | \beta - H \cdot log\left(\frac{d+\theta}{d_{24}+\theta}\right), \tau_\sigma^2\right) \times \\ N\left(\xi_d | \bar{\xi}, \tau_\xi^2\right) \times N\left(\alpha | 0, 10^6\right) \times N\left(\beta | 0, 10^6\right) \times \\ \mathrm{B}(H | 1, 1, 0, 1) \times U(\theta | 0, 10) \times N\left(\bar{\xi} | 0, 0.3^2\right) \times \\ Inv - Gamma\left(\tau_\mu^2 | 0.01, 0.01\right) \times Inv - Gamma\left(\tau_\sigma^2 | 0.01, 0.01\right) \times \\ Inv - Gamma\left(\tau_\xi^2 | 0.01, 0.01\right) \end{gathered} \quad (9)$$

where T is the number of years. The subscripts $d(d_{24} = 24)$ and j denote the rainfall duration and the year, respectively. α and β are $log(\mu_{24})$ and $log(\sigma_{24})$ respectively. H and θ are the scaling parameters. $\bar{\xi}$ is the average shape parameter across the considered rainfall durations. τ_μ^2, τ_σ^2, and, τ_ξ^2 denote the variance of GEV parameters in the scaling processes. $N(\cdot,\cdot)$ and $U(\cdot,\cdot)$ are the normal distribution and uniform distribution, respectively. $B(\cdot,\cdot,a,b)$ is the beta distribution with lower bound of a and upper bound of b. $Inv-Gamma(\cdot,\cdot)$ is the inverse gamma distribution with shape and scale parameters. The prior for $\bar{\xi}$ is a normal distribution with a standard deviation of 0.3 (Cheng et al., 2014). The priors for other parameters are explained in detail in Lima et al. (2018). To obtain the posterior distribution of the GEV parameters, we adopted the widely used Markov Chain Monte Carlo to sample from the posterior distribution of Eq. (9). We considered 20,000 iterations for each of five chains with the first 10,000 iterations discarded. A thinning rate of 50 was adopted to avoid serial dependence. The convergence of the posterior distributions was evaluated based on the $\widehat{R}$ coefficient (Lima et al., 2018). GEV parameters estimated based on Eq. (9) were then used to obtain the return rainfalls for the durations considered.

Historical return rainfalls at different durations were used to construct the historical IDF curves. However, future return rainfalls, which were based on future disaggregated MMS by ANN, could distort the true MMS. Fig. 5 displays a similar distortion (e.g., light-tail problems in shorter durations) in the historical period. When constructing future IDF curves, this distortion needs to be considered. Therefore, first, we generated ANN-based historical and future return rainfalls. Secondly, the 'change factor' (climate response that indicates the ratio of future rainfall intensities to historical ones) (Wilby et al., 2009) was computed by the ratio of ANN-based future return rainfalls to ANN-based historical ones. Finally, we constructed the IDF curves for future periods by multiplying the 'change factor' and observation-based historical return rainfalls (future IDF curves = observation-based IDF curves × future ANN-based IDF curves / historical ANN-based IDF curves). This procedure is similar to the development of IDF curves by using the ratio of model-based future rainfall intensity and model-based historical rainfall intensity in Liew et al. (2014) and Tabari et al. (2016).

4. Results and discussion

4.1. Comparison of NQM, QM, and QDM

Fig. 4 shows the total error of each dataset from CORDEX-SEA generated by the three BC methods. For each climate model dataset of CORDEX-SEA simulations, the most suitable BC method (either of QM, QDM, and NQM) was selected to minimize the total error integrating the influence of bias correction and CCS preservation. On the whole, we selected NQM, QDM, and QM as the most suitable BC method for downscaling 15, 11, and 2 rainfall datasets, respectively (this number corresponds to the number of black bars for each BC method shown in Fig. 4). This difference indicates that NQM and QDM performed better than QM. QM performed poorly mainly because QM uses the error correction values established at a higher ECDF to remove the bias at a lower ECDF, which could alter the raw modeled CCS (Switanek et al., 2017). The best BC methods remained almost the same in the near and far future periods and were similar in HCMC and CTC (Fig. 4). This similarity in selecting suitable BC methods for HCMC and CTC makes sense given the geographical location of these two cities.

In general, NQM and QDM performed better than QM. For some CORDEX-SEA products (e.g., far future case of Model 7 for HCMC), NQM gave a comparably small total error, although NQM was not selected as the best BC method. Given that NQM performed better than the other two BC methods with regard to certain datasets (e.g., No. 4 in Table 1), climate change impact studies in other cities are suggested to use NQM. In addition, since datasets downscaled by selected BC methods performed better than the datasets downscaled by one specific BC method, future study should consider selecting a suitable BC method for each climate model.

4.2. Disaggregated MMS

Table 2 shows that the optimum input variables for ANN-based models are the same between HCMC and CTC. Comparing AIC between the input variable with *sim_MMR*12 and without *sim_MMR*12, such as $(P_{t-1}, P_t, P_{t+1}, sim\_MMR12)$ and (P_{t-1}, P_t, P_{t+1}), we found that *sim_MMR*12 improved accuracy for long durations (i.e., MMR6, MMR18, MMR24) while reduced it for short durations (i.e., MMR1, MMR3). This finding is probably because that compared with long-duration rainfall extreme, short-duration rainfall extreme is more related to the small-scale convective events (Fowler et al., 2021). Thus the long-duration rainfall extreme doesn't help a lot in improving accuracy for the short durations. The best input variables (shown by the bold number) were then compared with Hyetosminute based on how well they reproduce the observed MMS (Fig. 5 and Fig. S1) and used to obtain future MMS for different durations. The evaluation of ANN-based models is listed in Table S1, where the models performed similarly on the training datasets and test datasets, which indicates that there are no overfitting and underfitting problems.

Fig. 5 and Fig. S1 compare the quantile–quantile plot of the observed and simulated (disaggregated) MMS. Both ANN-based model and

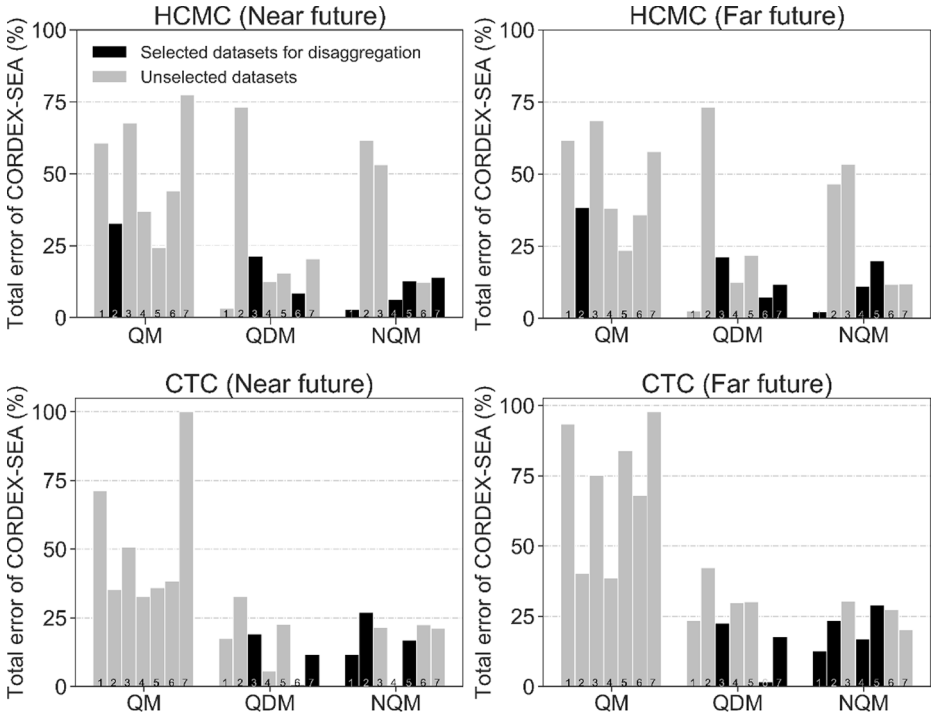

Fig. 4. Total error for datasets of CORDEX-SEA generated by three BC methods for HCMC (top) and CTC (bottom) in the near future and far future periods. The black bar indicates the minimum error among the three BC methods (QM, QDM, and NQM) for each dataset. The number at the bottom of each bar, 1 to 7, corresponds to the dataset number in Table 1.

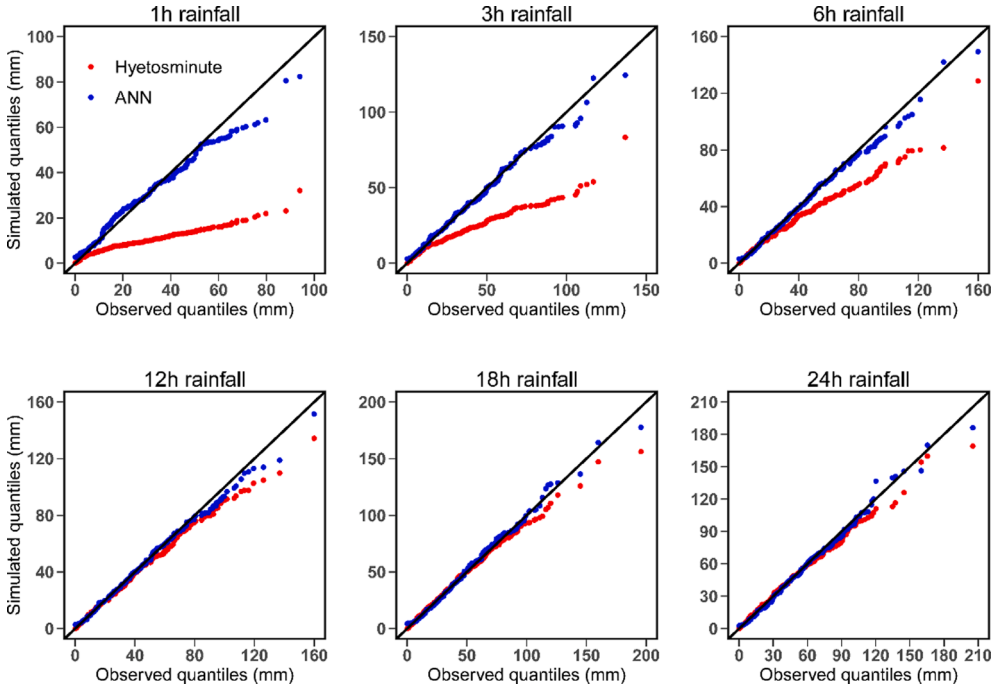

Fig. 5. Comparison of the quantile–quantile plot of the observed and disaggregated (wet-day) monthly maximum series in HCMC.

Hyetosminute gave satisfactory results in long durations (i.e., 12, 18, 24 h), while ANN-based model performed much better than Hyetosminute in short durations (i.e., 1, 3, 6 h). However, both ANN-based model and Hyetosminute tended to distort from (mainly underestimate) the observed MMS in the tails, especially in short durations. These results were in agreement with the results in Mirhosseini et al. (2014). Distortion problems are unavoidable, especially for short durations (Arnbjerg-Nielsen et al., 2013; Burian et al., 2000; Burian and Durrans, 2002; Kossieris et al., 2018; Mirhosseini et al., 2014). This is maybe because short-duration rainfalls are mainly derived from small-scale convective events (which usually last less than one day) that are difficult to represent by the daily rainfall datasets (Llasat, 2001).

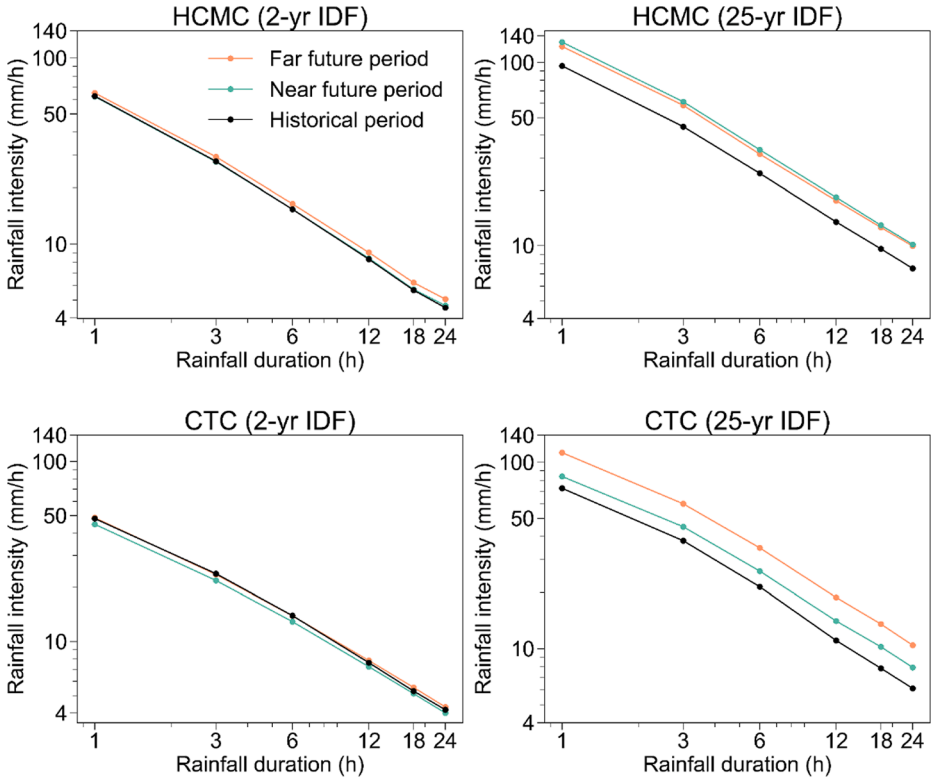

Fig. 6. 2 and 25-yr IDF curves for historical and future periods in HCMC (top) and CTC (bottom) based on observed and bias-corrected model datasets. IDF curves for future periods are the mean of the future projections based on the datasets (downscaled by selected BC methods) shown by black bars (after temporal disaggregation) in Fig. 4.

Although we improved the ANN-based model by using the most accurate outputs (i.e., *sim_MMR*12) in previous steps as the inputs in later steps, as shown in Table 2, we further need to reduce uncertainty in future studies. First, we can consider other climate factors (such as temperature) as input variables to improve the accuracy of results, especially in short durations. Mirhosseini et al. (2014) showed that ANN-based model has better accuracy when using temperature as the input. Second, data for short durations, provided by high-resolution convection-permitting climate models, can be used directly (Cannon and Innocenti, 2019; Kendon et al., 2017).

In general, ANN-based model showed superior performance over Hyetosminute in short durations, and future work should consider using more input variables and convection-permitting climate models to reduce uncertainty.

4.3. Historical and future IDF curves

Fig. 6 and Fig. S4 display the IDF curves in historical and future periods. Comparing the 25-yr IDF curves for the near and far future periods, HCMC shows a higher rainfall intensity in the near future while CTC shows a lower rainfall intensity in this period. This observation can be attributed to the discrepancies among the climate models in simulating the changes in rainfall extremes. Based on a preliminary analysis (not shown), most raw climate models indicate that rainfall extremes (average of annual maximum daily rainfall) in the far future are smaller than those in the near future around HCMC, while giving an opposite result around CTC. This contradiction between climate modes provided by CORDEX-SEA simulations has also been identified by Supari et al. (2020), Tangang et al. (2020, 2019, 2018), and Trinh-Tuan et al. (2019). Owing to the complex climate and terrain in SEA, simulating the local rainfalls by regional climate models is still challenging (Tangang et al., 2020). With further development of CORDEX-SEA simulations, the uncertainties resulting from these simulations could be reduced in future studies. Despite the uncertainty, some common conclusions with regard to both HCMC and CTC can be drawn; these are mentioned as follows.

In the near future, for 2-yr IDF curves, which comprise the median values of annual maximum rainfall for different rainfall durations, HCMC showed an average change of 0.6% and CTC of −5.8% compared to the rainfall intensities during the historical period. The changes are in general agreement with the changes in annual maximum daily rainfall in this region reported by Tangang et al. (2018). In the far future, based on the 2-yr IDF curves, the rainfall intensity was expected to increase by 7.7% in HCMC and 1.8% in CTC, which is similar to changes in annual maximum daily rainfall in Supari et al. (2020). Furthermore, based on the 25-yr IDF curves, the rainfall intensity was expected to increase by 34.5–36.8% (depending on the rainfall duration) in HCMC and by 15.7–30.4% in CTC in the near future, and 27.4–32.6% in HCMC, 55.4–72.8% in CTC in the far future. Thus, compared with IDF curves with a lower return period, IDF curves with a higher return period increased more from the historical period. This difference implies that the rainfall intensity for rarer rainfall events will intensify more in the future, which is similar to the results in Truong Ha, (2018), and in other regions like Europe and North America (Cannon and Innocenti, 2019; Kharin et al., 2018; Myhre et al., 2019). In addition to this observation, generally, more increase is found in longer-duration rainfall intensity in HCMC and CTC (Fig. S4). Despite the general increase, for some cases (e.g., 25-year in HCMC), longer-duration rainfall intensity increased less than that of shorter-duration one. This general increase compares well to a previous research on IDF curves in HCMC (Truong Ha, 2018). As extreme short-duration rainfall is generally responsible for flash flooding (Fowler et al., 2021), the less increase in extreme short-duration rainfall in our study region may be helpful in the timely implementation of efficient preventive measures for flash flooding.

Overall, rainfall intensity with higher return periods, especially for longer durations, is expected to increase more in both cities and future periods. These expected change in IDF curves urges us to update the existing drainage systems for higher return periods in HCMC and CTC.

4.4. Uncertainty in IDF curves

The IDF curves projected for the future period include different kinds of uncertainty due to the observed and modeled datasets, and the methods used to estimate the IDF curves.

The observed datasets collected by the rain gauges are affected by systematic errors such as the underestimation due to the wind effects, and evaporation (Hosseinzadehtalaei et al., 2020), which is difficult to verify for the observed data we used. In addition, the observations with a record length of 20 years are easily affected by the natural variability of the climate system (Aalbers et al., 2018), thus causing uncertainty in the estimated return rainfall. This limited record length of data is mainly due to the limited observation period and the setting of the historical period in CORDEX-SEA simulations, which ends in 2005. Since the period of projection under RCP scenarios starts from 2006, we constrain the time span of observed rainfall examined in this study to 1986–2005. Nevertheless, the applied Bayesian GEV model uses more information to estimate the return rainfall, leading to a reduction in uncertainty caused by the natural variability. The uncertainty in the climate models can be attributed to various factors in RCMs and GCMs (e.g., physical parameterization schemes, coarse spatial resolutions, and boundary forcing) (Tangang et al., 2019, 2020). In RCMs, modeling the convective rainfall poses certain errors in the estimation of rainfall. For example, the convective rainfall scheme used in RegCM4-3 (Table 1), i.e., MIT-Emanuel cumulus parameterization scheme, was found to generally overestimate daily rainfall amount (Tangang et al., 2020) and daily rainfall extremes (e.g., R99pTOT) over SEA (Ge et al., 2019), and some models (e.g., No.3 in Table 1) even projected an opposite future change compared with the forcing GCMs (Tangang et al., 2020). Regarding the temperature, RCMs simulated the daily temperature better than GCMs in our research area, but still projected a different temperature from the forcing GCMs in the future period (Nguyen-Thi et al., 2021). Generally, RCMs affect the return rainfall estimates (Fig. 7) much more than the forcing GCMs (Berg et al. 2019). In addition, the coarse spatial resolution of the RCMs is difficult to provide us the high-resolution local rainfall fields in an urban environment, especially in complex terrain (Poschlod et al., 2018). Obtaining local rainfall fields from these RCMs based on BC methods could also cause uncertainty. All these limitations in climate models would cause significant uncertainty in return rainfall estimates (Poschlod et al., 2021). As SEA could be more affected by the enhanced convectional process in the future (Ge et al., 2019), RCMs with explicit convection schemes (focusing on the spatial resolution of 3–4 km) are needed to improve the results (Tabari et al., 2016). In addition to the shortcomings of these climate models, the natural variability of the climate system also limits the predictability of the CCS indicated by the climate models (Aalbers et al., 2018). These effects of natural variability on rainfall were found more obvious at smaller spatial scales and shorter durations (Hawkins and Sutton, 2009; Aalbers et al., 2018). As these effects are difficult to estimate from observations with a limited record length, Poschlod et al. (2021) quantified their effects by using 50 ensemble members with the same emission scenario, model structure, and physics. Results show that the convectional process is more affected by natural variability. Therefore, it is also important to quantify the impact of natural variability on the estimated IDF curves, which is subject to the future work.

The uncertainty due to the choice of BC methods gives a substantial influence on the estimation of sub-daily rainfall extremes and resulting IDF curves. Fig. 7 and Fig. S3 display the uncertainty of projected return rainfall in the future periods. Day (BC) and Day (Raw) represent the daily return rainfall based on bias-corrected models and those based on raw climate models, respectively. To better compare these two kinds of return rainfall, we applied an areal reduction factor of 0.8 to Day (Raw) (Willems, 2013). However, the area reduction factor is usually site-dependent, which should not be seen as a reliable transformation of

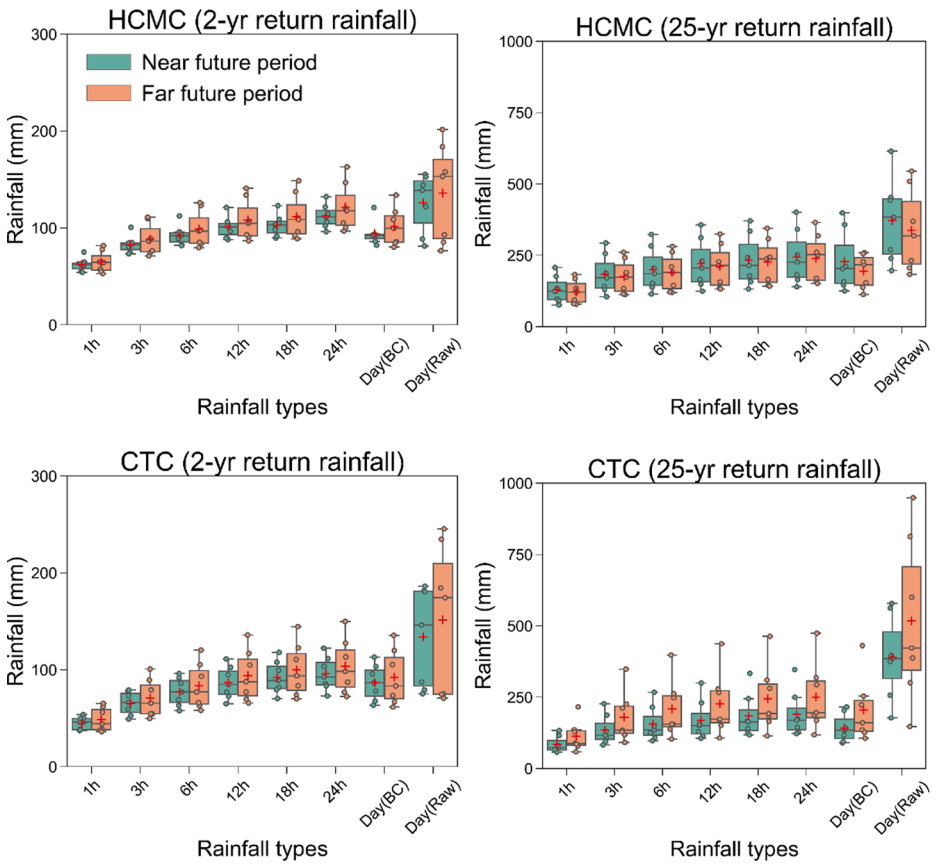

Fig. 7. Box plot showing the uncertainty in 2 and 25-yr return rainfalls with different rainfall durations in HCMC (top) and CTC (bottom). Day (BC) and Day (Raw) represent the daily return rainfall based on bias-corrected model datasets (downscaled by selected BC methods) and those divided by an areal reduction factor based on raw climate model datasets (that mean uncorrected models), respectively. The horizontal line within the box represents the median value, and each circle represents rainfall depth for a specific climate model. The red plus sign in the figure denotes the ensemble mean value. The extent of box signifies the first quartile (Q1) to the third quartile (Q3), which is also called interquartile range (IQR). The values outside the range of [Q1-1.5IQR, Q3 + 1.5IQR] are considered as outliers. (For interpretation of the references to colour in this figure legend, the reader is referred to the web version of this article.)

Day (Raw) (Poschlod et al., 2021). The range of the return rainfall (ensemble spread) is usually used as a measure of the uncertainty and ensemble median or mean (the former being more outlier-robust and the latter making full use of the obtained information) is advocated as a representation of the future (Kundzewicz et al., 2018). Maurer and Pierce (2014) found that after bias correction, the ensemble mean better preserved the raw modeled CCS than the ensemble median. This better performance based on the ensemble mean is also shown in Fig. 7, where the ensemble mean of Day (BC) showed a similar CCS (change from near future to far future) to that of Day (Raw), while ensemble median Day (BC) sometimes (e.g., 2-yr return rainfall in CTC) showed an opposite CCS to that of Day (Raw). Even though Fig. 7 displays some outliers in the certain boxplots (e.g., 1 h, 25-year return rainfall in CTC), these outliers (defined by the boxplot) also represent possible and plausible futures (Kundzewicz et al., 2018). Therefore, if we apply BC methods to remove the systematic model bias, using the ensemble mean instead of the ensemble median is suggested. The rainfall intensity change based on ensemble median is also provided as supplementary material (Table S2).

Compared with Day(Raw), Day(BC) decreased the ensemble spread of daily return rainfalls by 47.1% in HCMC and 61.4% in CTC. This decrease indicates that the BC methods used in our study (especially NQM and QDM) reduced the uncertainty caused by the systematic model bias effectively owing to their approach to capture the CCS, although BC methods cannot be used to solve the fundamental problems of RCMs (e.g., parameterization schemes) (Maraun, 2016). Furthermore, ensemble means of Day (Raw) generally gave a larger return rainfall than those of Day (BC). This overestimation in rainfall extremes was also reported by Supari et al. (2020). A preliminary analysis (not shown) shows that some models project extremely large rainfalls, which cannot be seen as outliers without a compelling reason. The bias in these larger rainfalls is difficult to remove by almost all BC methods that calculate quantiles in a non-parametric way (Maraun et al., 2019). Future work could use a parametric method (such as Generalized Pareto distribution) to fit these extremes in the bias correction (Switanek et al., 2017).

Some durations, such as 12, 18, and 24 h in CTC (Fig. 7, 25-yr return rainfall, near future), gave a wider ensemble spread than that of Day (BC). This wider spread is mainly due to the uncertainty arising from the temporal disaggregation model. This uncertainty from temporal disaggregation models cannot be eliminated (Burian et al., 2000; Burian and Durrans, 2002; Kossieris et al., 2018; Mirhosseini et al., 2014) but can be reduced by the solutions (i.e., using more input variables and convection-permitting climate models) mentioned in Section 4.2. Moreover, the temporal disaggregation model trained by the historical daily rainfall datasets was used in the future period based on the so-called stationarity assumption, which could introduce additional uncertainty. Although using the projected daily rainfall datasets for future periods reduces the uncertainty, the rainfall generating systems for the sub-daily rainfall are usually different from the daily rainfall (Cannon and Innocenti, 2019). Quantifying the uncertainty caused by the stationarity assumption is difficult due to the complexity of the rainfall generating systems and the interaction between thermodynamic and dynamic factors (Moustakis et al., 2021). Though the stationarity assumption is commonly accepted in climate change impact studies (Hosseinzadehtalaei et al., 2020, 2021; Lombardo et al., 2017), this assumption needs to be checked in the future study when climate models with higher accuracy are available (Berg et al., 2019).

5. Conclusion

This study provides a framework for constructing IDF curves in the near future period (2026–2045) and far future period (2066–2085) for tropical cities in Southeast Asia based on the state of art climate models provided by CORDEX-SEA simulations, through the application in two cities in Southern Vietnam. In this framework, we proposed a new BC method, NQM, and compared it with QDM and QM. Furthermore, we

selected the best BC method for each dataset provided by CORDEX-SEA to ensure the removal of the systematic model biases by BC methods as well as the retainment of the raw modeled CCS of CORDEX-SEA simulations. An ANN-based disaggregation model was introduced and compared with a stochastic disaggregation model, Hyetosminute. The following conclusions can be drawn:

(1) In general, NQM and QDM performed better than QM. Given that for some datasets, NQM showed much better accuracy than QDM and QM, the climate change impact studies in other cities should consider using NQM and comparing it with other downscaling methods.
(2) CORDEX-SEA-simulated rainfall is always characterized by a significant bias and uncertainty, which precludes its direct use for constructing IDF curves. The selected BC methods eliminated the systematic model bias and reduced the associated model uncertainty for the construction of IDF curves for future periods effectively.
(3) The short-duration MMS generated by ANN was much more accurate than that generated by Hyetosminute. Future work should focus on reducing uncertainty, especially in short durations. In addition to utilizing the enhanced observed and modeled datasets, using the most accurate outputs in previous steps as the inputs in later steps is recommended.
(4) Projected IDF curves for future periods revealed that rainfall intensity for rarer rainfall events was expected to increase more, especially for longer durations, requiring that the existing urban drainage systems for higher return periods in HCMC and CTC be updated.

CRediT authorship contribution statement

Wenpeng Zhao: Conceptualization, Data curation, Methodology, Software, Validation, Formal analysis, Investigation, Visualization, Writing - original draft. **Tsuyoshi Kinouchi:** Funding acquisition, Data curation, Supervision, Writing - review & editing. **Hong Quan Nguyen:** Resources, Data curation.

Declaration of Competing Interest

The authors declare that they have no known competing financial interests or personal relationships that could have appeared to influence the work reported in this paper.

Acknowledgement

This research is funded by the Japan Society for the Promotion of Science (JSPS) Bilateral Joint Research Program. The first author acknowledges the financial support from the China Scholarship Council (CSC). Authors acknowledge the World Climate Research Programme's Working Group on Regional Climate, and the Working Group on Coupled Modelling, former coordinating body of CORDEX and responsible panel for CMIP5. Authors thank ICTP, GERICS, SMHI for producing and making their model simulations available.

Appendix A. Supplementary data

Supplementary data to this article can be found online at https://doi.org/10.1016/j.jhydrol.2021.126461.

References

Aalbers, E.E., Lenderink, G., van Meijgaard, E., van den Hurk, B.J.J.M., 2018. Local-scale changes in mean and heavy precipitation in Western Europe, climate change or internal variability? Clim. Dyn. 50, 4745–4766. https://doi.org/10.1007/s00382-017-3901-9.

Arnbjerg-Nielsen, K., Willems, P., Olsson, J., Beecham, S., Pathirana, A., Bülow Gregersen, I., Madsen, H., Nguyen, V.-T.-V., 2013. Impacts of climate change on rainfall extremes and urban drainage systems: a review. Water Sci. Technol. 68, 16–28. https://doi.org/10.2166/wst.2013.251.

Berg, P., Christensen, O.B., Klehmet, K., Lenderink, G., Olsson, J., Teichmann, C., Yang, W., 2019. Summertime precipitation extremes in a EURO-CORDEX 0.11° ensemble at an hourly resolution. Nat. Hazards Earth Syst. Sci. 19, 957–971. https://doi.org/10.5194/nhess-19-957-2019.

Blanchet, J., Ceresetti, D., Molinié, G., Creutin, J.D., 2016. A regional GEV scale-invariant framework for Intensity–Duration–Frequency analysis. J. Hydrol. 540, 82–95. https://doi.org/10.1016/j.jhydrol.2016.06.007.

Burian, S.J., Durrans, S.R., 2002. Evaluation of an artificial neural network rainfall disaggregation model. Water Sci. Technol. 45, 99–104. https://doi.org/10.2166/wst.2002.0033.

Burian, S.J., Durrans, S.R., Tomić, S., Pimmel, R.L., Wai, C.N., 2000. Rainfall disaggregation using artificial neural networks. J. Hydrol. Eng. 5, 299–307. https://doi.org/10.1061/(ASCE)1084-0699(2000)5:3(299).

Cannon, A.J., Innocenti, S., 2019. Projected intensification of sub-daily and daily rainfall extremes in convection-permitting climate model simulations over North America: implications for future intensity–duration–frequency curves. Nat. Hazards Earth Syst. Sci. 19, 421–440. https://doi.org/10.5194/nhess-19-421-2019.

Cannon, A.J., Sobie, S.R., Murdock, T.Q., 2015. Bias correction of GCM precipitation by quantile mapping: How well do methods preserve changes in quantiles and extremes? J. Clim. 28, 6938–6959. https://doi.org/10.1175/JCLI-D-14-00754.1.

Cannon, A.J., 2018. Multivariate quantile mapping bias correction: an N-dimensional probability density function transform for climate model simulations of multiple variables. Clim. Dyn. 50, 31–49. https://doi.org/10.1007/s00382-017-3580-6.

Chen, J., Brissette, F.P., Chaumont, D., Braun, M., 2013a. Finding appropriate bias correction methods in downscaling precipitation for hydrologic impact studies over North America. Water Resour. Res. 49, 4187–4205. https://doi.org/10.1002/wrcr.20331.

Chen, J., Brissette, F.P., Chaumont, D., Braun, M., 2013b. Performance and uncertainty evaluation of empirical downscaling methods in quantifying the climate change impacts on hydrology over two North American river basins. J. Hydrol. 479, 200–214. https://doi.org/10.1016/j.jhydrol.2012.11.062.

Chen, J., Chen, H., Guo, S., 2018. Multi-site precipitation downscaling using a stochastic weather generator. Clim. Dyn. 50, 1975–1992. https://doi.org/10.1007/s00382-017-3731-9.

Chen, J., Zhang, X.J., Brissette, F.P., 2014. Assessing scale effects for statistically downscaling precipitation with GPCC model. Int. J. Climatol. 34, 708–727. https://doi.org/10.1002/joc.3717.

Cheng, L., AghaKouchak, A., Gilleland, E., Katz, R.W., 2014. Non-stationary extreme value analysis in a changing climate. Clim. Change 127, 353–369. https://doi.org/10.1007/s10584-014-1254-5.

Coles, S., Bawa, J., Trenner, L., Dorazio, P., 2001. An Introduction to Statistical Modeling of Extreme Values, vol. 208. Springer.

Endreny, T.A., Imbeah, N., 2009. Generating robust rainfall intensity-duration-frequency estimates with short-record satellite data. J. Hydrol. 371, 182–191. https://doi.org/10.1016/j.jhydrol.2009.03.027.

Fowler, H.J., Lenderink, G., Prein, A.F., Westra, S., Allan, R.P., Ban, N., Barbero, R., Berg, P., Blenkinsop, S., Do, H.X., Guerreiro, S., Haerter, J.O., Kendon, E.J., Lewis, E., Schaer, C., Sharma, A., Villarini, G., Wasko, C., Zhang, X., 2021. Anthropogenic intensification of short-duration rainfall extremes. Nat. Rev. Earth Environ. https://doi.org/10.1038/s43017-020-00128-6.

Ge, F., Zhu, S., Peng, T., Zhao, Y., Sielmann, F., Fraedrich, K., Zhi, X., Liu, X., Tang, W., Ji, L., 2019. Risks of precipitation extremes over Southeast Asia: Does 1.5 °c or 2 °c global warming make a difference? Environ. Res. Lett. 14 https://doi.org/10.1088/1748-9326/aaff7e.

F. Giorgi C. Jones G.R. Asrar et al. Addressing climate information needs at the regional level: the CORDEX framework World Meteorological Organization (WMO) Bulletin. Available from < 2009 https://public.wmo.int/en/bulletin/addressing-climate-information-needs-regional-level-cordex-framework>.

Gudmundsson, L., Bremnes, J.B., Haugen, J.E., Engen-Skaugen, T., 2012. Technical Note: Downscaling RCM precipitation to the station scale using statistical transformations – a comparison of methods. Hydrol. Earth Syst. Sci. 16, 3383–3390. https://doi.org/10.5194/hess-16-3383-2012.

Gutowski, W.J., Giorgi, F., 2020. Coordination of Regional Downscaling. Oxford Res. Encycl. Clim. Sci. https://doi.org/10.1093/acrefore/9780190228620.013.658.

Hausfather, Z., Peters, G.P., 2020. Emissions - the "business as usual" story is misleading. Nature 577, 618–620.

Hawkins, E., Sutton, R., 2009. The potential to narrow uncertainty in regional climate predictions. Bull. Am. Meteorol. Soc. 90, 1095–1108. https://doi.org/10.1175/2009BAMS2607.1.

He, X., Chaney, N.W., Schleiss, M., Sheffield, J., 2016. Spatial downscaling of precipitation using adaptable random forests. Water Resour. Res. 52, 8217–8237. https://doi.org/10.1002/2016WR019034.

Hewitson, B., Crane, R., 1996. Climate downscaling: techniques and application. Clim. Res. 7, 85–95. https://doi.org/10.3354/cr007085.

Hijioka, Y., Lin, E., Pereira, J.J., Corlett, R.T., Cui, X., Insarov, G.E., Lasco, R.D., Lindgren, E., Surjan, A., 2014. Asia. Climate Change 2014: Impacts, Adaptation, and Vulnerability. Part B: Regional Aspects. Contribution of Working Group II to the Fifth Assessment Report of the Intergovernmental Panel on Climate Change, Cambridge University Press, Cambridge, United Kingdom and New York. Available from <https://www.ipcc.ch/site/assets/uploads/2018/02/WGIIAR5-Chap24_FINAL.pdf>.

Hnilica, J., Hanel, M., Puš, V., 2017. Multisite bias correction of precipitation data from regional climate models. Int. J. Climatol. 37, 2934–2946. https://doi.org/10.1002/joc.4890.

Hoegh-Guldberg, O., Jacob, D., Bindi, M., Brown, S., Camilloni, I., Diedhiou, A., Djalante, R., Ebi, K., Engelbrecht, F., Guiot, J., Others, 2018. Impacts of 1.5°C Global Warming on Natural and Human Systems. In: Global Warming of 1.5°C. An IPCC Special Report on the impacts of global warming of 1.5°C above pre-industrial levels and related global greenhouse gas emission pathways, in the context of strengthening the global response to the threat of climate change, sustainable development, and efforts to eradicate poverty, Special Report, Intergovernmental Panel on Climate Change. Available from <https://www.ipcc.ch/site/assets/uploads/sites/2/2019/02/SR15_Chapter3_Low_Res.pdf>.

Hosseinzadehtalaei, P., Ishadi, N.K., Tabari, H., Willems, P., 2021. Climate change impact assessment on pluvial flooding using a distribution-based bias correction of regional climate model simulations. J. Hydrol. 598, 126239 https://doi.org/10.1016/j.jhydrol.2021.126239.

Hosseinzadehtalaei, P., Tabari, H., Willems, P., 2020. Climate change impact on short-duration extreme precipitation and intensity–duration–frequency curves over Europe. J. Hydrol. 590, 125249 https://doi.org/10.1016/j.jhydrol.2020.125249.

Huong, H.T.L., Pathirana, A., 2013. Urbanization and climate change impacts on future urban flooding in Can Tho city. Vietnam. Hydrol. Earth Syst. Sci. 17, 379–394. https://doi.org/10.5194/hess-17-379-2013.

Ivanov, M.A., Kotlarski, S., 2017. Assessing distribution-based climate model bias correction methods over an alpine domain: added value and limitations. Int. J. Climatol. 37, 2633–2653. https://doi.org/10.1002/joc.4870.

Johnson, F., Sharma, A., 2012. A nesting model for bias correction of variability at multiple time scales in general circulation model precipitation simulations. Water Resour. Res. 48, 1–16. https://doi.org/10.1029/2011WR010464.

Kendon, E.J., Ban, N., Roberts, N.M., Fowler, H.J., Roberts, M.J., Chan, S.C., Evans, J.P., Fosser, G., Wilkinson, J.M., 2017. Do convection-permitting regional climate models improve projections of future precipitation change? Bull. Am. Meteorol. Soc. 98, 79–93. https://doi.org/10.1175/BAMS-D-15-0004.1.

Kharin, V.V., Flato, G.M., Zhang, X., Gillett, N.P., Zwiers, F., Anderson, K.J., 2018. Risks from climate extremes change differently from 1.5°C to 2.0°C depending on rarity. Earth's Futur. 6, 704–715. https://doi.org/10.1002/2018EF000813.

Kossieris, P., Makropoulos, C., Onof, C., Koutsoyiannis, D., 2018. A rainfall disaggregation scheme for sub-hourly time scales: coupling a Bartlett-Lewis based model with adjusting procedures. J. Hydrol. 556, 980–992. https://doi.org/10.1016/j.jhydrol.2016.07.015.

Koutsoyiannis, D., 2003. Rainfall disaggregation methods: Theory and applications, in: Proceedings,Workshop on Statistical and Mathematical Methods for Hydrological Analysis. Università Degli Studi Di Roma "La Sapienza, Rome, pp. 1–23. https://doi.org/https://doi.org/10.13140/RG.2.1.2840.8564.

Koutsoyiannis, D., Kozonis, D., Manetas, A., 1998. A mathematical framework for studying rainfall intensity-duration-frequency relationships. J. Hydrol. 206, 118–135. https://doi.org/10.1016/S0022-1694(98)00097-3.

Koutsoyiannis, D., Onof, C., 2001. Rainfall disaggregation using adjusting procedures on a Poisson cluster model. J. Hydrol. 246, 109–122. https://doi.org/10.1016/S0022-1694(01)00363-8.

Kundzewicz, Z.W., Krysanova, V., Benestad, R.E., Hov, Piniewski, M., Otto, I.M., 2018. Uncertainty in climate change impacts on water resources. Environ. Sci. Policy 79, 1–8. https://doi.org/10.1016/j.envsci.2017.10.008.

Li, X., Babovic, V., 2019. Multi-site multivariate downscaling of global climate model outputs: an integrated framework combining quantile mapping, stochastic weather generator and Empirical Copula approaches. Clim. Dyn. 52, 5775–5799. https://doi.org/10.1007/s00382-018-4480-0.

Li, Z., Shi, X., Li, J., 2017. Multisite and multivariate GCM downscaling using a distribution-free shuffle procedure for correlation reconstruction. Clim. Res. 72, 141–151. https://doi.org/10.3354/cr01460.

Y. Li D.B.A. Jones C.M. Zarzycki Evaluating the Performance of VR-CESM for Modeling Precipitation in Southeast Asia GESM Working Group Meetings. Available from 2019 <https://www.cesm.ucar.edu/events/wg-meetings/2019/presentations/AMWGChemWAWG/li.pdf>.

Liew, S.C., Raghavan, S.V., Liong, S.Y., 2014. How to construct future IDF curves, under changing climate, for sites with scarce rainfall records? Hydrol. Process. 28, 3276–3287. https://doi.org/10.1002/hyp.9839.

Lima, C.H.R., Kwon, H.H., Kim, Y.T., 2018. A local-regional scaling-invariant Bayesian GEV model for estimating rainfall IDF curves in a future climate. J. Hydrol. 566, 73–88. https://doi.org/10.1016/j.jhydrol.2018.08.075.

Llasat, M.-C., 2001. An objective classification of rainfall events on the basis of their convective features: application to rainfall intensity in the northeast of spain. Int. J. Climatol. 21, 1385–1400. https://doi.org/10.1002/joc.692.

Lombardo, F., Volpi, E., Koutsoyiannis, D., Serinaldi, F., 2017. A theoretically consistent stochastic cascade for temporal disaggregation of intermittent rainfall. Water Resour. Res. 53, 4586–4605. https://doi.org/10.1002/2017WR020529.

Lu, Y., Qin, X.S., 2014. Multisite rainfall downscaling and disaggregation in a tropical urban area. J. Hydrol. 509, 55–65. https://doi.org/10.1016/j.jhydrol.2013.11.027.

Macukow, B., 2016. Neural networks–state of art, brief history, basic models and architecture, in: IFIP International Conference on Computer Information Systems and Industrial Management. pp. 3–14. Available from https://hal.inria.fr/hal-01637477/document.

Maraun, D., 2016. Bias correcting climate change simulations - a critical review. Curr. Clim. Chang. Reports 2, 211–220. https://doi.org/10.1007/s40641-016-0050-x.

Maraun, D., 2013. Bias correction, quantile mapping, and downscaling: revisiting the inflation issue. J. Clim. 26, 2137–2143. https://doi.org/10.1175/JCLI-D-12-00821.1.

Maraun, D., Wetterhall, F., Ireson, A.M., Chandler, R.E., Kendon, E.J., Widmann, M., Brienen, S., Rust, H.W., Sauter, T., Themeßl, M., Venema, V.K.C., Chun, K.P., Goodess, C.M., Jones, R.G., Onof, C., Vrac, M., Thiele-Eich, I., 2010. Precipitation downscaling under climate change: recent developments to bridge the gap between dynamical models and the end user. Rev. Geophys. 48, RG3003. https://doi.org/10.1029/2009RG000314.

Maraun, D., Widmann, M., Gutiérrez, J.M., 2019. Statistical downscaling skill under present climate conditions: a synthesis of the VALUE perfect predictor experiment. Int. J. Climatol. 39, 3692–3703. https://doi.org/10.1002/joc.5877.

Marra, F., Morin, E., 2015. Use of radar QPE for the derivation of Intensity-Duration-Frequency curves in a range of climatic regimes. J. Hydrol. 531, 427–440. https://doi.org/10.1016/j.jhydrol.2015.08.064.

Marra, F., Morin, E., Peleg, N., Mei, Y., Anagnostou, E.N., 2017. Intensity-duration-frequency curves from remote sensing rainfall estimates: comparing satellite and weather radar over the eastern Mediterranean. Hydrol. Earth Syst. Sci. 21, 2389–2404. https://doi.org/10.5194/hess-21-2389-2017.

Maurer, E.P., Pierce, D.W., 2014. Bias correction can modify climate model simulated precipitation changes without adverse effect on the ensemble mean. Hydrol. Earth Syst. Sci. 18, 915–925. https://doi.org/10.5194/hess-18-915-2014.

Mehrotra, R., Sharma, A., 2016. A multivariate quantile-matching bias correction approach with auto- and cross-dependence across multiple time scales: implications for downscaling. J. Clim. 29, 3519–3539. https://doi.org/10.1175/JCLI-D-15-0356.1.

Mehrotra, R., Sharma, A., 2015. Correcting for systematic biases in multiple raw GCM variables across a range of timescales. J. Hydrol. 520, 214–223. https://doi.org/10.1016/j.jhydrol.2014.11.037.

Mélèse, V., Blanchet, J., Molinié, G., 2018. Uncertainty estimation of Intensity–Duration–Frequency relationships: a regional analysis. J. Hydrol. 558, 579–591. https://doi.org/10.1016/j.jhydrol.2017.07.054.

Mendenhall, J., Meiler, J., 2016. Improving quantitative structure–activity relationship models using Artificial Neural Networks trained with dropout. J. Comput. Aided. Mol. Des. 30, 177–189. https://doi.org/10.1007/s10822-016-9895-2.

Mirhosseini, G., Srivastava, P., Fang, X., 2014. Developing rainfall intensity-duration-frequency curves for alabama under future climate scenarios using artificial neural networks. J. Hydrol. Eng. 19, 04014022. https://doi.org/10.1061/(ASCE)HE.1943-5584.0000962.

Mirhosseini, G., Srivastava, P., Stefanova, L., 2013. The impact of climate change on rainfall Intensity-Duration-Frequency (IDF) curves in Alabama. Reg. Environ. Chang. 13, 25–33. https://doi.org/10.1007/s10113-012-0375-5.

Moustakis, Y., Papalexiou, S.M., Onof, C.J., Paschalis, A., 2021. Seasonality, intensity, and duration of rainfall extremes change in a warmer climate. Earth's Futur. 9, 1–15. https://doi.org/10.1029/2020EF001824.

Mullan, D., Chen, J., Zhang, X.J., 2016. Validation of non-stationary precipitation series for site-specific impact assessment: comparison of two statistical downscaling techniques. Clim. Dyn. 46, 967–986. https://doi.org/10.1007/s00382-015-2626-x.

Muller, A., Bacro, J.N., Lang, M., 2008. Bayesian comparison of different rainfall depth-duration-frequency relationships. Stoch. Environ. Res. Risk Assess. 22, 33–46. https://doi.org/10.1007/s00477-006-0095-9.

Müller, H., Haberlandt, U., 2018. Temporal rainfall disaggregation using a multiplicative cascade model for spatial application in urban hydrology. J. Hydrol. 556, 847–864. https://doi.org/10.1016/j.jhydrol.2016.01.031.

Myhre, G., Alterskjær, K., Stjern, C.W., Hodnebrog, Ø., Marelle, L., Samset, B.H., Sillmann, J., Schaller, N., Fischer, E., Schulz, M., Stohl, A., 2019. Frequency of extreme precipitation increases extensively with event rareness under global warming. Sci. Rep. 9, 16063. https://doi.org/10.1038/s41598-019-52277-4.

Ngai, S.T., Juneng, L., Tangang, F., Chung, J.X., Salimun, E., Tan, M.L., Amalia, S., 2020. Future projections of Malaysia daily precipitation characteristics using bias correction technique. Atmos. Res. 240, 104926 https://doi.org/10.1016/j.atmosres.2020.104926.

Nguyen-Thi, T., Ngo-Duc, T., Tangang, F.T., Cruz, F., Juneng, L., Santisirisomboon, J., Aldrian, E., Phan-Van, T., Narisma, G., 2021. Climate analogue and future appearance of novel climate in Southeast Asia. Int. J. Climatol. 41, E392–E409. https://doi.org/10.1002/joc.6693.

Nourani, V., Farboudfam, N., 2019. Rainfall time series disaggregation in mountainous regions using hybrid wavelet-artificial intelligence methods. Environ. Res. 168, 306–318. https://doi.org/10.1016/j.envres.2018.10.012.

Panchal, G., Ganatra, A., Kosta, Y.P., Panchal, D., 2010. Searching most efficient neural network architecture using akaike's information criterion (AIC). Int. J. Comput. Appl. 1, 54–57. https://doi.org/10.5120/126-242.

Papalexiou, S.M., Koutsoyiannis, D., Makropoulos, C., 2013. How extreme is extreme? An assessment of daily rainfall distribution tails. Hydrol. Earth Syst. Sci. 17, 851–862. https://doi.org/10.5194/hess-17-851-2013.

Peleg, N., Marra, F., Fatichi, S., Paschalis, A., Molnar, P., Burlando, P., 2018. Spatial variability of extreme rainfall at radar subpixel scale. J. Hydrol. 556, 922–933. https://doi.org/10.1016/j.jhydrol.2016.05.033.

Poschlod, B., Hodnebrog, Ø., Wood, R.R., Alterskjær, K., Ludwig, R., Myhre, G., Sillmann, J., 2018. Comparison and evaluation of statistical rainfall disaggregation and high-resolution dynamical downscaling over complex terrain. J. Hydrometeorol. 19, 1973–1982. https://doi.org/10.1175/JHM-D-18-0132.1.

Poschlod, B., Ludwig, R., Sillmann, J., 2021. Ten-year return levels of sub-daily extreme precipitation over Europe. Earth Syst. Sci. Data 13, 983–1003. https://doi.org/10.5194/essd-13-983-2021.

Rajagopalan, B., Salas, J.D., Lall, U., 2010. STOCHASTIC METHODS FOR MODELING PRECIPITATION AND STREAMFLOW, in: Advances in Data-Based Approaches for Hydrologic Modeling and Forecasting. WORLD SCIENTIFIC, pp. 17–52. https://doi.org/10.1142/9789814307987_0002.

Räty, O., Räisänen, J., Ylhäisi, J.S., 2014. Evaluation of delta change and bias correction methods for future daily precipitation: intermodel cross-validation using ENSEMBLES simulations. Clim. Dyn. 42, 2287–2303. https://doi.org/10.1007/s00382-014-2130-8.

Roelfsema, M., van Soest, H.L., Harmsen, M., van Vuuren, D.P., Bertram, C., den Elzen, M., Höhne, N., Iacobuta, G., Krey, V., Kriegler, E., Luderer, G., Riahi, K., Ueckerdt, F., Després, J., Drouet, L., Emmerling, J., Frank, S., Fricko, O., Gidden, M., Humpenöder, F., Huppmann, D., Fujimori, S., Fragkiadakis, K., Gi, K., Keramidas, K., Köberle, A.C., Aleluia Reis, L., Rochedo, P., Schaeffer, R., Oshiro, K., Vrontisi, Z., Chen, W., Iyer, G.C., Edmonds, J., Kannavou, M., Jiang, K., Mathur, R., Safonov, G., Vishwanathan, S.S., 2020. Taking stock of national climate policies to evaluate implementation of the Paris Agreement. Nat. Commun. 11, 2096. https://doi.org/10.1038/s41467-020-15414-6.

Sharma, A., Mehrotra, R., 2010. Rainfall generation, in: Geophysical Monograph Series. pp. 215–246. https://doi.org/10.1029/2010GM000973. Available from <https://agupubs.onlinelibrary.wiley.com/doi/10.1029/2010GM000973>.

Sharma, A., Srikanthan, S., 2006. Continuous rainfall simulation: a nonparametric alternative, in: 30th Hydrology \& Water Resources Symposium: Past, Present \& Future. p. 86. Available from <https://search.informit.org/doi/10.3316/INFORMIT.499059223202660>.

Srivastav, R.K., Schardong, A., Simonovic, S.P., 2014. Equidistance quantile matching method for updating IDF curves under climate change. Water Resour. Manag. 28, 2539–2562. https://doi.org/10.1007/s11269-014-0626-y.

Su, T., Chen, J., Cannon, A.J., Xie, P., Guo, Q., 2020. Multi-site bias correction of climate model outputs for hydro-meteorological impact studies: an application over a watershed in China. Hydrol. Process. 34, 2575–2598. https://doi.org/10.1002/hyp.13750.

Shen, C., Laloy, E., Elshorbagy, A., Albert, A., Bales, J., Chang, F.-J., Ganguly, S., Hsu, K.-L., Kifer, D., Fang, Z., Fang, K., Li, D., Li, X., Tsai, W.-P., 2018. HESS opinions: incubating deep-learning-powered hydrologic science advances as a community. Hydrol. Earth Syst. Sci. 22, 5639–5656. https://doi.org/10.5194/hess-22-5639-2018.

Supari, Tangang, F., Juneng, L., Cruz, F., Chung, J.X., Ngai, S.T., Salimun, E., Mohd, M.S. F., Santisirisomboon, J., Singhruck, P., PhanVan, T., Ngo-Duc, T., Narisma, G., Aldrian, E., Gunawan, D., Sopaheluwakan, A., 2020. Multi-model projections of precipitation extremes in Southeast Asia based on CORDEX-Southeast Asia simulations. Environ. Res. 184, 109350. https://doi.org/10.1016/j.envres.2020.109350.

Switanek, M.B., Troch, P.A., Castro, C.L., Leuprecht, A., Chang, H.-I., Mukherjee, R., Demaria, E.M.C., 2017. Scaled distribution mapping: a bias correction method that preserves raw climate model projected changes. Hydrol. Earth Syst. Sci. 21, 2649–2666. https://doi.org/10.5194/hess-21-2649-2017.

Tabari, H., 2020. Climate change impact on flood and extreme precipitation increases with water availability. Sci. Rep. 10, 1–10. https://doi.org/10.1038/s41598-020-70816-2.

Tabari, H., De Troch, R., Giot, O., Hamdi, R., Termonia, P., Saeed, S., Brisson, E., Van Lipzig, N., Willems, P., 2016. Local impact analysis of climate change on precipitation extremes: are high-resolution climate models needed for realistic simulations? Hydrol. Earth Syst. Sci. 20, 3843–3857. https://doi.org/10.5194/hess-20-3843-2016.

Tabari, H., Hosseinzadehtalaei, P., AghaKouchak, A., Willems, P., 2019. Latitudinal heterogeneity and hotspots of uncertainty in projected extreme precipitation. Environ. Res. Lett. 14, 124032 https://doi.org/10.1088/1748-9326/ab55fd.

Tangang, F., Chung, J.X., Juneng, L., Supari, Salimun, E., Ngai, S.T., Jamaluddin, A.F., Mohd, M.S.F., Cruz, F., Narisma, G., Santisirisomboon, J., Ngo-Duc, T., Van Tan, P., Singhruck, P., Gunawan, D., Aldrian, E., Sopaheluwakan, A., Grigory, N., Remedio, A.R.C., Sein, D. V., Hein-Griggs, D., McGregor, J.L., Yang, H., Sasaki, H., Kumar, P., 2020. Projected future changes in rainfall in Southeast Asia based on CORDEX–SEA multi-model simulations. Clim. Dyn. 55, 1247–1267. https://doi.org/10.1007/s00382-020-05322-2.

Tangang, F., Santisirisomboon, Jerasorn, Juneng, L., Salimun, E., Chung, J., Supari, S., Cruz, F., Ngai, S.T., Ngo-Duc, T., Singhruck, P., Narisma, G., Santisirisomboon, Jaruthat, Wongsaree, W., Promjirapawat, K., Sukamongkol, Y., Srisawadwong, R., Setsirichok, D., Phan-Van, T., Aldrian, E., Gunawan, D., Nikulin, G., Yang, H., 2019. Projected future changes in mean precipitation over Thailand based on multi-model regional climate simulations of CORDEX Southeast Asia. Int. J. Climatol. 39, 5413–5436. https://doi.org/10.1002/joc.6163.

Tangang, F., Supari, S., Chung, J.X., Cruz, F., Salimun, E., Ngai, S.T., Juneng, L., Santisirisomboon, Jerasorn, Santisirisomboon, Jaruthat, Ngo-Duc, T., Phan-Van, T., Narisma, G., Singhruck, P., Gunawan, D., Aldrian, E., Sopaheluwakan, A., Nikulin, G., Yang, H., Remedio, A.R.C., Sein, D., Hein-Griggs, D., 2018. Future changes in annual precipitation extremes over Southeast Asia under global warming of 2°C. APN Sci. Bull. 8. https://doi.org/10.30852/sb.2018.436.

Themeßl, M.J., Gobiet, A., Heinrich, G., 2012. Empirical-statistical downscaling and error correction of regional climate models and its impact on the climate change signal. Clim. Change 112, 449–468. https://doi.org/10.1007/s10584-011-0224-4.

Trenberth, K.E., Dai, A., Rasmussen, R.M., Parsons, D.B., 2003. The changing character of precipitation. Bull. Am. Meteorol. Soc. 84, 1205–1218. https://doi.org/10.1175/BAMS-84-9-1205.

Trinh-Tuan, L., Matsumoto, J., Tangang, F.T., Juneng, L., Cruz, F., Narisma, G., Santisirisomboon, J., Phan-Van, T., Gunawan, D., Aldrian, E., Ngo-Duc, T., 2019. Application of Quantile Mapping bias correction for mid-future precipitation projections over Vietnam. Sci. Online Lett. Atmos. 15, 1–6. https://doi.org/10.2151/SOLA.2019-001.

Truong Ha, M., 2018. Climate Change Impact on Intensity-Duration-Frequency Curves in Ho Chi Minh city, In: Workshop on Disaster Resilient Cities. Available from < http://ancst.org/wp-content/uploads/2018/07/4.-Mr.-Minh-Truong-Ha-Vietnam-Institute-of-Meteorology-Hydrology-and-Climate-Change.pdf>.

Trzaska, S., Schnarr, E., 2014. A review of downscaling methods for climate change projections, United States Agency for International Development by Tetra Tech ARD. Available from <http://www.ciesin.org/documents/Downscaling_CLEARED_000.pdf>.

Vachaud, G., Quertamp, F., Phan, T.S.H., Tran Ngoc, T.D., Nguyen, T., Luu, X.L., Nguyen, A.T., Gratiot, N., 2019. Flood-related risks in Ho Chi Minh City and ways of mitigation. J. Hydrol. 573, 1021–1027. https://doi.org/10.1016/j.jhydrol.2018.02.044.

Volosciuk, C., Maraun, D., Vrac, M., Widmann, M., 2017. A combined statistical bias correction and stochastic downscaling method for precipitation. Hydrol. Earth Syst. Sci. 21, 1693–1719. https://doi.org/10.5194/hess-21-1693-2017.

Wang, L., Ranasinghe, R., Maskey, S., van Gelder, P.H.A.J.M., Vrijling, J.K., 2016. Comparison of empirical statistical methods for downscaling daily climate projections from CMIP5 GCMs: a case study of the Huai River Basin. China. Int. J. Climatol. 36, 145–164. https://doi.org/10.1002/joc.4334.

Wilby, R.L., Troni, J., Biot, Y., Tedd, L., Hewitson, B.C., Smith, D.M., Sutton, R.T., 2009. A review of climate risk information for adaptation and development planning. Int. J. Climatol. 29, 1193–1215. https://doi.org/10.1002/joc.1839.

Willems, P., 2013. Revision of urban drainage design rules after assessment of climate change impacts on precipitation extremes at Uccle. Belgium. J. Hydrol. 496, 166–177. https://doi.org/10.1016/j.jhydrol.2013.05.037.

Xu, Z., Han, Y., Yang, Z., 2019. Dynamical downscaling of regional climate: a review of methods and limitations. Sci. China Earth Sci. 62, 365–375. https://doi.org/10.1007/s11430-018-9261-5.